

Modelling mass transfer from a packed bed by fluid extraction

Timothy G. Myers^{a,1}, Abel Valverde^b, Maria Aguares^c, Marc Calvo-Schwarzwalder^d,
Francesc Font^{a,e}

^a*Centre de Recerca Matemàtica, Campus de Bellaterra, Edifici C, 08193 Bellaterra, Barcelona, Spain*

^b*Department of Chemical Engineering, ETSEIB, UPC, Diagonal 647, 08028, Barcelona, Spain*

^c*Department of Computer Science, Applied Mathematics and Statistics, Universitat de Girona, Campus de Montilivi, 17071 Girona, Catalunya, Spain*

^d*College of Natural and Health Sciences, Zayed University, PO Box 144534 Abu Dhabi, United Arab Emirates*

^e*Department of Fluid Mechanics, Universitat Politècnica de Catalunya - BarcelonaTech, Barcelona 08019, Spain*

Abstract

A mathematical model describing the erosion or leaching of a solid material by a flowing fluid in a column is developed. This involves an advection-diffusion equation coupled to a linear kinetic reaction describing the mass transfer between the solid and fluid. Two specific cases are analysed, the first where the extracted material has the same saturation solubility and rate of mass transfer throughout the process, the second where the solubility switches after a certain amount of erosion. In the first case there are only two model unknowns, the solubility and mass transfer coefficient, in the second there is a third unknown, the second solubility. Exploiting the fact that erosion is a slow process (relative to the flow rate) a perturbation solution based on the smallness of the amount removed is developed to describe the concentration and radius throughout the column. From this an analytical expression for the extracted fraction is obtained. The extracted fraction has a large linear section which results in a simple calculation to estimate the initial solubility from a very few or even a single data point. The remaining unknowns may also be easily calculated from the formula and later data points. A numerical solution, using finite differences, is developed to verify the perturbation solution. The analytical solution is also verified against experimental data for the removal of lanolin from wool fibres with a supercritical CO₂/ethanol solvent. Values for the mass transfer rate and two solubilities are obtained for different pressures and shown to provide excellent agreement with a series of experimental results for the extracted fraction.

Keywords: Advection-diffusion equations; Supercritical fluid extraction; Moving boundary problems; Perturbation methods; Mathematical model; Sorption column.

1. Introduction

The extraction of a material which is somehow attached to or embedded in a solid by the action of a flowing fluid has countless applications in both nature and industry. Erosive processes occur naturally whilst many essential oils are produced through desorption caused by the injection of solvent. In manufacturing processes solvent driven extraction is a widely used

¹Corresponding author: tmyers@crm.cat

technique. In the review of [1] a variety of examples of solvent extraction are described, including from leaves, seeds, roots, mushrooms and even cow brains. Essential oils, produced via extraction techniques, are used in areas such as food, pharmaceutical, cosmetic or perfume industries [2], natural dyes in the textile industry [3] or natural components for medical applications [4]. Lanolin, which coats sheep wool, has applications in pharmaceuticals, cosmetics, coatings, rust-proofing and moustache wax [5, 6]. Alongside the range of extracts there is also a variety of solvents. In recent years supercritical fluids have come to the fore for reasons of cost, non-flammability, toxicity or availability, especially when compared to other commonly used petroleum-based solvents such as hexane or benzene [4, 7, 8, 9, 10, 11, 12].

The basic mathematical framework for extraction or erosion consists of a mass balance for the extract within the solvent coupled to a transfer model between the solid and solvent. In the context of column extraction various forms of this framework may be found in the literature, from coupling two differential equations [13], coupled mass balances in both the solid and fluid phases [7, 14, 15, 16, 17] to accounting for a moving solid-fluid interface representing the desorption of the material into the solvent [18, 19, 20, 21, 22, 23, 24]. Solutions are invariably numerical, via some form of discretization [14, 15, 21, 23, 18] or a polynomial approximation [19]. However, some simple analytical approximations have been presented which involve the neglect of spatial variation [7, 24] (so variables depend only on time). An extensive review of models can be found in [1].

Many mathematical models analogous to those describing extraction may be found in the literature of deposition processes, for example, in the removal from fluids containing emerging contaminants, volatile organic compounds, CO₂, dyes and salts [25, 26]. While the chemistry may be radically different to extraction the difference in mathematical models may be as simple as a change of sign in the mass source/sink term. Consequently, there is the possibility of knowledge transfer from this field while the results of the present study may be adapted to aid in the understanding of contaminant removal.

As is the nature of models all involve degrees of approximation and assumptions, such as averaging over the column cross-section, neglect of thermal effects or assuming negligible amounts of extract so that the solvent properties and flow are unaffected. Certain assumptions are based on solid physical grounds while others are motivated by a desire to obtain a tractable model. In a study of contaminant removal by adsorption [27, 28] rather than starting from accepted models the authors started from the basic conservation laws, rigorously identifying negligible terms and justifying all assumptions made, with the result that a number of errors in accepted models were identified. It was discussed how these errors can lead to problems in determining system parameters and, importantly, in the scaling-up of experiments. The corrected model of [27, 28] removed many of the issues caused by these errors.

In the current study we will take the same approach as [27, 28], starting from conservation of mass and then non-dimensionalising to identify dominant and negligible terms. To keep the model general certain standard assumptions are avoided. One such assumption is that the amount extracted is small compared to the total solid mass: neglecting this assumption leads to a variation of particle radius, void fraction and velocity along the column. For cases where the amount extracted is indeed small compared to the solid the model reduces to a more standard form. During the development of the mathematical model we make no assumption on the type of solvent or solid material. However in the results section we will verify the model against experimental data for the removal of lanolin from wool via a supercritical CO₂-ethanol fluid.

2. Derivation of governing equations

We begin by stating a number of assumptions made in the development of the present model:

1. The concentration/density of material attached to the core remains constant throughout the process.
2. This material is attached to the outside of the core rather than being contained within a porous media. In this way the reduction of solid area is directly related to mass removal.
3. The mass removed is much less than the mass of liquid passed through the column (but may be of a similar order to the amount of solid available for extraction).
4. The inlet mass flux is constant.

The first assumption is consistent with a process where the solvent does not diffuse into the material to be removed, so there exists a sharp boundary between the two. This approach is employed in the shrinking core model of [21]. The second assumption is valid for the processes of interest in this study, where the material to be extracted surrounds a solid core. Of course there are situations where the material is also inside a solid, porous core, for example in the Broken Intact Cell (BIC) model of [7]. The present model could be adapted to this situation, where the mass transfer rate depends on where material is extracted. In §6 we deal with a two solubility model, where the radius changes with time for both solubilities. A BIC type model is a simplified version of this, where the radius is fixed for the second solubility phase. The third assumption is consistent with a standard extraction, erosion or leaching processes. All are slow processes so that the concentration of removed material within the carrier fluid must always be small. Taking the example of [19, 29] a typical result involves the removal of 3g lanolin with more than 3kg solvent. Since the volume fraction of eroded material is of the order one thousandth that of the solvent it will have a negligible effect on solvent properties, such as density and viscosity. The final assumption is related to the experimental setup, whereby a flow meter controls the mass flux. An alternative approach could be to use a fixed pressure drop system, where the flux then varies as material is eroded. We will not investigate this latter situation.

2.1. Derivation of the general equations

To specify the model we consider a packed bed with a constant inner profile. It is filled with a coated material where the inner part of the material, denoted the core, maintains a constant volume while the coating is slowly removed. The total internal cross-sectional area is A_b^* , where $*$ indicates a dimensional quantity. The solid material is our main object of interest. It comprises the core and its coating and occupies a cross-sectional area A^* which is split into a constant area occupied by the core A_c^* and a variable area A_e^* consisting of the material to be removed; hence $A_e^* + A_c^* = A^*$. The void area A_v^* is such that $A^* + A_v^* = A_b^*$. The configuration is depicted in Figure 1a. The notation used in the paper as well as the subscripts to identify where the values are defined are given in Table 1.

The process is such that solvent entering at the inlet, $x^* = 0$, is free of the material to be removed. Moving along the bed the solvent slowly picks up small amounts of material until it either becomes saturated or exits the bed. Due to the mixing caused by the presence of numerous, randomly packed solids, radial variation is small so that properties such as the concentration may be taken to vary purely with distance from the inlet and time, $c^* = c^*(x^*, t^*)$.

Table 1: Notation and key subscripts used in this work.

Parameters

A^*	Cross-sectional area (m ²)
M^*	Mass per unit length (kg/m)
M_{tot}^*	Total mass available for extraction (kg)
c^*	Concentration density of eroded material (kg/m ³)
x^*	Distance from the column inlet (m)
L^*	Length of the bed (m)
t^*	Time (s)
u^*	Flow velocity (m/s)
R^*	Average radius of the core plus coating (m)
ρ^*	Density (kg/m ³)
ϵ	Void fraction
D^*	Mass diffusivity (m ² /s)
k^*	Kinetic or mass transfer coefficient (m/s)
\dot{m}^*	Mass flux of solvent (kg/s)
X^*	Extracted fraction

Subscripts

b	Bed or column	i	Initial value
c	Core material	s	Solvent
e	Material available for extraction	v	Void

This approach is analogous to applying an averaging process over the cross-section. Since the packing is random the cross-sectional area will vary along the column, even at $t^* = 0$, consequently we must think of the variables as a form of ensemble average, that is, an average taken over various cross-sections. The extraction from the solid has consequences for a number of quantities. Erosion corresponds to mass loss from the solid and so $A_e^* = A_e^*(x^*, t^*)$. Since the core and bed areas are fixed $A^*(x^*, t^*) = A_c^* - A_e^*(x^*, t^*)$, $A_v^*(x^*, t^*) = A_b^* - A^*(x^*, t^*)$ are variable. Then the void fraction $\epsilon(x^*, t^*) = A_v^*(x^*, t^*)/A_b^*$ is also a variable quantity. Finally, with a varying void region conservation of mass dictates that the interstitial velocity $u^* = u^*(x^*, t^*)$.

A straight-forward mass balance for the eroded material in the solvent over any given cross-section leads to

$$\frac{\partial M^*}{\partial t^*} + \frac{\partial}{\partial x^*}(u^* M^*) = \frac{\partial}{\partial x^*} \left(D^* \frac{\partial M^*}{\partial x^*} \right) - \frac{\partial M_e^*}{\partial t^*}. \quad (1)$$

Equation (1) states that the mass of eroded material within the solvent varies due to advection, diffusion and the rate at which eroded material enters the fluid. The mass per unit length, M^* , may be defined in terms of the concentration, c^* , of eroded material in the solvent $M^* = A_v^* c^* = \epsilon A_b^* c^*$. The diffusion coefficient depends on the void fraction and so is also variable.

The total mass of material per unit length available for extraction is denoted M_e^* where

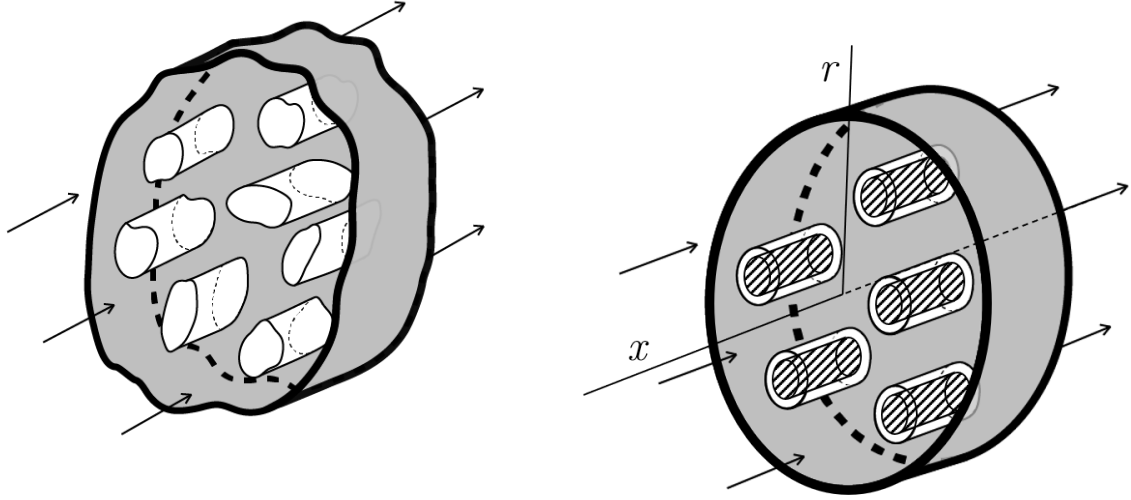


Figure 1: On the left, the diagram showing a cross-section of an arbitrary profile experimental setup. On the right, the circular cross-section column and solids considered in §2.2. The total bed circular area is A_b^* , the grey area inside the bed is the void area, A_v^* , the white area in the cylinders is the area available for extraction, A_e^* , and the striped area is the core, A_c^* .

$\partial M_e^*/\partial t^* \leq 0$. If ρ_e^* is the constant density of this material when attached to the core then

$$M_e^* = \rho_e^* A_e^* \quad \Rightarrow \quad \frac{\partial M_e^*}{\partial t^*} = \rho_e^* \frac{\partial A_e^*}{\partial t^*}. \quad (2)$$

The extraction process may also be considered in terms of a kinetic reaction. Assuming a linear form we may write

$$\frac{\partial M_e^*}{\partial t^*} = -k^*(c_s^* - c^*)\delta A_e^*, \quad (3)$$

where δA_e^* represents the total boundary of the solid area available for the reaction (or in this case mass transfer) and c_s^* is the saturation concentration. The kinetic coefficient k^* provides information about the extraction rate. This will vary with the ambient conditions. Both k^* , c_s^* are usually unknown.

As stated in §2 a lot of solvent is required to remove small amounts of material, so the solvent mass flux is much greater than the flux of eroded material. Consequently we may state that the interstitial velocity

$$u^*(x^*, t^*) = \frac{\dot{m}^*}{\rho_s^* \epsilon(x^*, t^*) A_b^*}, \quad (4)$$

where \dot{m}^* is the mass flux of solvent and ρ_s^* the solvent density. For future reference we observe that the product ϵu^* is constant provided \dot{m}^* is constant. If \dot{m}^* varies with time then the product ϵu^* is also a function of time.

In order to proceed we must define the typical shape of the bed and solid. The reason for this being that the mass balance is in terms of an area while the kinetic reaction depends on the surface exposed to solvent, which is the boundary of the solid material. The relation between

the solid area and its boundary depends on the shape. In Figure 1a) we depict a deliberately random shape. Bed shapes can take a variety of forms while extraction from leaves, flowers, peel etc will involve many forms of solid cross-section. Fibres aligned along the bed axis will have a circular cross-section but if they are not aligned with the bed walls or are subject to bending the cross-section will be non-circular.

A common simplification is to think in terms of equivalent solid materials with a circular cross-section and then to determine an average radius depending on the void fraction. We will follow this approach in the following section and further assume a circular cross-section bed.

2.2. Circular cross-section bed and solid

From now on we will focus on a circular cross-section bed, with internal radius R_b^* since this is the most common shape studied in the literature. In terms of the solid area it is standard to work in terms of an average radius, circular cross-section material, as depicted in Figure 1b). If a typical column cross-section contains n solid components which occupy a fraction $(1 - \epsilon)$ then the average radius of the core material plus the coating, R^* , is defined through

$$A^* = (1 - \epsilon)\pi R_b^{*2} = n\pi R^{*2}. \quad (5)$$

The radius of the core is denoted R_c^* .

Since n is constant we may rearrange the above expression to define it in terms of the initial values and also to relate the void fraction $\epsilon(x^*, t^*)$ to the bed and solid areas

$$n = \frac{(1 - \epsilon(x^*, t^*))R_b^{*2}}{R^{*2}(x^*, t^*)} = \frac{(1 - \epsilon_i)R_b^{*2}}{R_i^{*2}}, \quad (6)$$

$$\epsilon(x^*, t^*) = 1 - n \frac{R^{*2}(x^*, t^*)}{R_b^{*2}} = 1 - (1 - \epsilon_i) \frac{R^{*2}(x^*, t^*)}{R_i^{*2}}, \quad (7)$$

where subscript i indicates the initial value and it is assumed that $R^*(x^*, 0) = R_i^*$, $\epsilon(x^*, 0) = \epsilon_i$ are constant throughout the column. The mass available for extraction may now be written

$$M_e^*(x^*, t^*) = \rho_e^* A_e^* = \rho_e^* n\pi (R^{*2} - R_c^{*2}). \quad (8)$$

Since the area of the core is constant

$$\frac{\partial M_e^*}{\partial t^*} = 2\rho_e^* n\pi R^* \frac{\partial R^*}{\partial t^*}, \quad (9)$$

determines the source term. For extraction the radius decreases with time, hence $\partial R^*/\partial t^* < 0$.

The kinetic reaction involves the boundary of the solid material and so from (3) we may write

$$\frac{\partial M_e^*}{\partial t^*} = -k^* 2n\pi R^* (c_s^* - c^*), \quad (10)$$

where $2n\pi R^*$ is the surface area (per unit length) of the solid available for the reaction/mass transfer. This holds whenever $c^* \leq c_s^*$, $R^* \geq R_c^*$ that is extraction stops if the fluid becomes saturated or when all available material has been removed from the core. Equating the two mass loss expressions gives

$$\frac{\partial R^*}{\partial t^*} = -\frac{k^*}{\rho_e^*} (c_s^* - c^*). \quad (11)$$

The mass per unit length of extracted material in the fluid may be written as $M^* = \epsilon \pi R_b^2 c^*$ then, after noting that R_b^* is constant, the mass balance (1) becomes

$$\begin{aligned} \frac{\partial}{\partial t^*}(\epsilon c^*) + \frac{\partial}{\partial x^*}(u^* \epsilon c^*) &= \frac{\partial}{\partial x^*} \left(D^* \frac{\partial}{\partial x^*}(\epsilon c^*) \right) - \frac{1}{\pi R_b^{*2}} \frac{\partial M_e^*}{\partial t^*} \\ &= \frac{\partial}{\partial x^*} \left(D^* \frac{\partial}{\partial x^*}(\epsilon c^*) \right) + \frac{2nk^*}{R_b^{*2}} R^*(c_s^* - c^*), \end{aligned} \quad (12)$$

where the mass source is defined by either of equations (9,10), here we have taken the latter, and ϵ satisfies (7). In comparison a typical model from the literature takes the form

$$\epsilon \frac{\partial c^*}{\partial t^*} + \epsilon u^* \frac{\partial c}{\partial x^*} = \epsilon D^* \frac{\partial^2 c^*}{\partial x^{*2}} + k^* \Gamma^*(c_s^* - c^*), \quad (13)$$

where Γ^* represents a constant surface area parameter. The form of equation (13) corresponds, for example, to the ‘new’ model of [23], the ‘general fluid phase mass balance’ in the review of [24] (after correcting for an error in the time derivative and converting from superficial to interstitial velocity), the ‘shrinking core model’ of [21] and many others.

Comparison of (12, 13) clearly demonstrates key differences such as

1. The variation of ϵ, u^*, D^* requires these quantities to be included within the derivative terms. Their dependence on R^* makes the equations nonlinear and hence significantly more complex to solve.
2. The source term in (13) is expressed in terms of a specified, constant surface area, from (12) we see it is proportional to $R^*(x^*, t^*)$ and so variable, providing another source of nonlinearity.

To close the system requires boundary and initial conditions. Initially no material has been extracted and the column is filled with a fluid that does not act as a solvent. The first condition may be stated as $R^*(x^*, 0) = R_i^*$. For the second we may apply various options. First, we could treat this as a moving boundary problem where no initial condition is imposed on c^* since there is no eroded material within the column. For $t > 0$ we then have an interface at $x^* = u_i^* t^*$, behind this there is solvent and we neglect the region ahead of the interface. Only when solvent reaches the outlet do we apply the system throughout the column. An alternative approach, which permits an initial condition, would be to treat the liquid within the column at $t^* = 0$ as a saturated fluid since it does not result in any extraction, i.e. define $c^*(x^*, 0) = c_s^*$. This prevents the mathematical model from predicting extraction before solvent passes through the column. If we were to naively write $c^*(x^*, 0) = 0$, to indicate there is no solvent in the column, then at $t^* = 0$ the model would indicate that liquid already in the column would immediately erode material everywhere (and at the fastest rate possible).

As a consequence of the R^* condition we may define $\epsilon(x^*, 0) = \epsilon_i^* = 1 - nR_i^{*2}/R_b^{*2}$. Since the incoming solvent is free of eroded material, $c^*(0^-, t^*) = 0$ continuity of flux at the inlet requires

$$0 = \left(u^* \epsilon c^* - D^* \frac{\partial}{\partial x^*}(\epsilon c^*) \right) \Big|_{x^*=0^+}. \quad (14)$$

In the limit where $D^* \rightarrow 0$ this may be simplified to $c^*(0, t^*) = 0$. This inlet condition is based on an assumption that extraction is occurring in the vicinity of the inlet. However, if the solid

material is stripped, such that $R^* = R_c^*$, then extraction only occurs for positions $x^* > s^*(t^*)$ where beyond $x^* = s^*(t^*)$ there remains material available for extraction $R^* > R_c^*$. In which case for $x^* \geq s^*(t^*)$ we apply

$$c^*(s^*(t^*), t^*) = 0, \quad R^*(s^*(t^*), t^*) = R_c^*. \quad (15)$$

For $x^* \leq s^*(t^*)$ functions take the constant values $c^*(x^*, t^*) = 0, R^*(x^*, t^*) = R_c^*$.

The diffusion term of (12) is second order thus requiring a second boundary condition on concentration. However, since advection dominates over diffusion and so information is advected in the positive x direction this condition will have little effect on the results. The full condition at the outlet should involve matching the flux expression across the boundary. However at the outlet the form of the flow is not clear and will depend on the particular experimental setup. Consequently here we assume that whatever the concentration on leaving the column it remains the same just outside the exit and impose

$$\frac{\partial c^*}{\partial x^*}(L^*, t^*) = 0. \quad (16)$$

Effectively this condition indicates zero diffusive flux at the outlet, which is consistent with the fact advection dominates over diffusion, this will become apparent in the non-dimensional analysis below. The neglect of the diffusive flux then raises the question why, if diffusion is generally negligible, include it in the inlet condition? The reason being that at the start of the process the clean fluid enters at the inlet and encounters a porous matrix packed with the maximum amount of material available for extraction. The concentration gradient will therefore take its greatest value at early times at the inlet and this is when diffusion may play a significant role. The same cannot be said for the outlet where the fluid containing the extracted material exits the column and the extraction process ends, changes across this boundary will therefore be small. In §4 we verify this showing that the early time solution has an outlet gradient approximately 0.005 smaller than the inlet gradient. A second verification is provided in the results section by the close agreement between the perturbation solution (which neglects diffusion and hence only employs the inlet condition) and the full numerical solution.

2.3. Extracted fraction

The extracted fraction refers to the mass of extracted material passing through the outlet at a given time divided by the total amount of material initially available for extraction. It is thus a dimensionless quantity varying between 0 and 1. However, as it will be conveniently scaled in §3 along with other relevant quantities, we will refer to it using the $*$ notation. Here we define the extracted fraction as

$$X^*(t^*) = \frac{\int_0^{t^*} u^* M^*(L^*, t^*) dt^*}{M_{tot}^*} = \frac{\epsilon_i u_i^* A_b^* \int_0^{t^*} c^*(L^*, t^*) dt^*}{M_{tot}^*}, \quad (17)$$

where we have used the fact $\epsilon u^* = \epsilon_i u_i^*$ is constant and the total mass available for extraction is denoted M_{tot}^* . If the initial distribution of mass is constant then $M_{tot}^* = M_e^*(x^*, 0)L^*$ otherwise

$$M_{tot}^* = \int_0^{L^*} M_e^*(x^*, 0) dx^*. \quad (18)$$

Subject to the circular cross-section model we have $M_{tot}^* = \rho_e^* n \pi (R_i^{*2} - R_c^{*2}) L^*$. Equivalently we may simply write down the available mass when provided from experimental data.

An alternative would be to define the extracted fraction in terms of the mass actually extracted during the experiment in which case the denominator of (17) matches the numerator but with the upper bound of the integral replaced by t_f^* , where t_f^* represents the time at which the experiment ends. This form accounts for the material actually extracted, which may not be the same as the available material. In the following we will use (17) with $M_{tot}^* = \rho_e^* n \pi (R_i^{*2} - R_c^{*2}) L^*$.

3. Non-dimensional form

We begin by scaling quantities with appropriate values

$$x = \frac{x^*}{\mathcal{L}^*}, \quad t = \frac{t^*}{\tau^*}, \quad u = \frac{u^*}{u_i^*}, \quad c = \frac{c^*}{c_s^*}, \quad R = \frac{R^*}{R_i^*}, \quad X = \frac{M_{tot}^* X^*}{\epsilon_i u_i^* A_b^* c_s^* \tau^*}, \quad D = \frac{D^*}{D_i^*}. \quad (19)$$

The void fraction is already non-dimensional and of order unity, so we make no scaling. The scaling of the particle radius is chosen so that the radius is now $R \in [R_c, 1]$, where $R_c = R_c^*/R_i^*$ is the scaled radius of the fiber core. The interstitial velocity scale is chosen from the initial inlet flux $u_i^* = \dot{m}^*/(\epsilon_i \rho_s^* \pi R_b^{*2})$. Although the extracted fraction is a non-dimensional quantity we impose the above scaling to simplify the form of expression.

In the new variables, the change in radius gives

$$\frac{\partial R}{\partial t} = -\frac{k^* c_s^* \tau^*}{\rho_e^* R_i^*} (1 - c) = -(1 - c), \quad (20)$$

provided we choose $\tau^* = \rho_e^* R_i^*/(k^* c_s^*)$. This corresponds to working on the time-scale of extraction, as opposed to the flow time-scale. The non-dimensional mass balance for the eroded material is

$$\frac{\mathcal{L}^*}{u_i^* \tau^*} \frac{\partial}{\partial t} (\epsilon c) + \frac{\partial}{\partial x} (u \epsilon c) = \frac{D_i^*}{\mathcal{L}^* u_i^*} \frac{\partial}{\partial x} \left(D \frac{\partial}{\partial x} (\epsilon c) \right) + \frac{2nk^* \mathcal{L}^* R_i^*}{R_b^{*2} u_i^*} R (1 - c), \quad (21)$$

where the quantities $\mathcal{L}^*/(u_i^* \tau^*)$ and $D_i^*/(\mathcal{L}^* u_i^*)$ represent the ratio of the extraction rate to the advective mass flow rate and the relative importance of diffusion to advection and thus they can be respectively classified as a form of Damköhler number, Da, and the inverse Peclet number Pe^{-1} . Upon identifying the length-scale over which the extraction takes place as $\mathcal{L}^* = u_i^* R_b^{*2}/(2nk^* R_i^*) = R_i^* u_i^*/(2(1-\epsilon_i)k^*)$ and noting that for a fixed inlet flux $\epsilon u = \epsilon_i$, (21) becomes

$$\text{Da} \frac{\partial}{\partial t} (\epsilon c) + \epsilon_i \frac{\partial c}{\partial x} = \text{Pe}^{-1} \frac{\partial}{\partial x} \left(D \frac{\partial}{\partial x} (\epsilon c) \right) + R (1 - c). \quad (22)$$

We may replace ϵ via the nondimensional form of equation (7),

$$\epsilon = 1 - (1 - \epsilon_i) R^2, \quad (23)$$

so that equation (22) now involves only the two primary unknowns, c, R . These may be determined via the two equations (20, 22). They are subject to

$$\left(\epsilon_i c - \text{Pe}^{-1} D \frac{\partial}{\partial x} (\epsilon c) \right) \Big|_{x=0} = 0, \quad \frac{\partial c}{\partial x} (L, t) = 0, \quad R(x, 0) = 1. \quad (24)$$

As discussed in the previous section the early time concentration may be treated as a moving boundary problem, neglecting c altogether at $t = 0$ since initially there is no solvent within the column or by setting $c(x, 0) = 1$ so that the fluid initially within the column causes no extraction (by imitating a saturated fluid). When a part of the solid is stripped, for $x \geq s(t)$, we solve (20, 22) subject to

$$\left(\epsilon_i c - \text{Pe}^{-1} D \frac{\partial}{\partial x} (\epsilon c) \right) \Big|_{x=s(t)} = 0, \quad R(s(t), t) = R_c. \quad (25)$$

For $x \leq s(t)$ functions take the constant values $c(x, t) = 0, R(x, t) = R_c$.

The extracted fraction is now

$$X = \int_0^t c(L, t) dt. \quad (26)$$

As will be seen later, when we introduce physical parameters the Damköhler number and inverse Peclet number are small, indicating that the dominant balance in equation (22) is between advection and extraction. The solution will then be well approximated using only these two terms (this is demonstrated more formally in the following section and appendix). However, this balance is inconsistent with the boundary condition at the exit $c_x(L, t) = 0$ indicating the presence of a boundary layer there, a small region where diffusion plays an important role. This will be discussed when the numerical results are presented.

4. Approximate solution method

Extraction is a slow process (in comparison to the flow rate) while mass transfer by diffusion is invariably small in comparison to fluid motion. Typically only a small fraction of the total solid region is removed during the process, which means that the final fibre radius is close to the initial value, $R_c^* \sim R_i^*$. Consequently we anticipate $\text{Da}, \text{Pe}^{-1} \ll 1 - R_c^*/R_i^* \ll 1$ (see the values shown in (66) for the application considered in Section §6). In this section we exploit the difference in scales to derive approximate expressions for the radius of the fibres, the concentration of the solid in the solvent, the void fraction in the column and the total extracted mass.

We shall consider two commonly encountered scenarios: one in which the saturation concentration remains the same throughout the process and a second in which the material to be extracted is composed of two different fractions, with two different saturation concentrations. The first is obviously the most common, and simplest to model, where a single solubility material coats the solid matrix. The second occurs, for example, with lanolin. The experimental results presented in [29] clearly demonstrate two different solubilities where the first fraction contains the light esters and free alcohols while the second has the higher molecular weight products. The solubility of the second being significantly lower than that of the first. The Broken-Intact Cell (BIC) model of Sovová [7] deals with extraction from a milled material where cells that have been opened by the milling have easily accessible material which is removed first, subsequently there is a slower extraction of material protected by the intact cell walls.

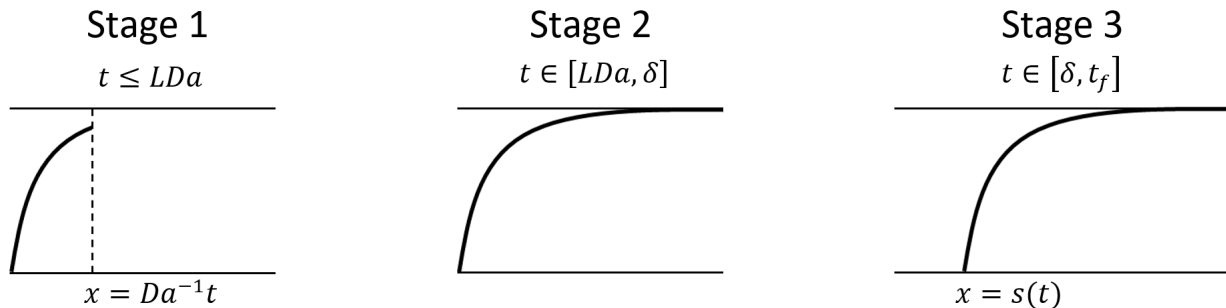


Figure 2: Representation of the evolution of the concentration during the three stages of the extraction process for a single solubility material.

4.1. Single solubility model

In the single solubility model the material is extracted in three stages, as depicted in Figure 2. Approximate expressions for the concentration and radius during each stage are given below. Details of their derivation are provided in Appendix A.1 where a perturbation method is used based on the smallness of the parameter $\delta = 1 - R_c^*/R_i^* = 1 - R_c \ll 1$. Taking only the leading order, *i.e.* neglecting δ altogether, will lead to errors of order δ while including terms of order δ leads to errors of order δ^2 (in fact the application of boundary conditions, which force the perturbation to match the exact solution at the boundaries, means that errors are often much smaller than indicated by the size of neglected terms). So, for example, if $R_c^* = 0.9R_i^*$ such that $\delta = 0.1$ then the leading order results in errors of order 10% while the first order errors will be of order 1%.

Stage 1. At very small times the clean solvent starts to flow through the column but there has not been sufficient time for it to reach the outlet. An interface exists between the solvent and fluid initially occupying the column. Beyond the interface no extraction has occurred and the void fraction is $\epsilon = \epsilon_i$. This indicates that the interface moves with velocity $u = 1$ (*i.e.* $u^* = u_i^*$). So, during Stage 1, solvent occupies the region $x \in [0, t/\text{Da}]$ (*i.e.* $x^* \in [0, u_i^*t^*]$). Solvent reaches the end of the column at time $t = t_1 = L\text{Da}$ ($t_1^* = L^*/u_i^*$). Since extraction is slow we assume that this occurs before all soluble material has been eroded at the inlet (this will be verified later when we deal with a concrete example in Section §6).

Stage 2. Solvent now occupies the whole column. This stage continues until all soluble material has been removed at the inlet, that is for $t \in [L\text{Da}, t_2]$, where $t_2 = \delta = 1 - R_c$ is the time required for the radius to reduce from 1 to R_c . Noting that $t_2 = \delta \ll 1$ we observe that these early stages occupy a small amount of the total process time.

Approximate solutions for the concentration and the radius during Stages 1 and 2 are given by

$$c_e(x, t) = (1 - e^{-x/\epsilon_i})(1 - te^{-x/\epsilon_i}), \quad R_e(x, t) = 1 - te^{-x/\epsilon_i}, \quad (27)$$

where δ does not appear explicitly due to a rescaling of time carried out in the appendix. We have denoted these solutions by c_e, R_e since they represent the early time behaviour, $0 < t \leq t_2$. In Stage 1, $t \in [0, t_1]$, these expressions hold over the region $x \in [0, t/\text{Da}]$, while for $x \geq t/\text{Da}$ there is no solvent (so the initial values apply). For Stage 2, $t \in [t_1, t_2]$, equation (27) holds over the whole column and this lasts until time $t_2 = \delta$ ($t_2^* = \delta\tau$).

Stage 3. The inlet material has been stripped and the point where $R^* = R_c^*$ now progresses through the column until all soluble material has been removed. Except very close to time $t = t_2$ the solution in this stage may be approximated by a travelling wave. Behind the wave $c = 0, R = R_c$, in front the solution to first order is

$$\begin{aligned} c_l(x, t) &= (1 - e^{-x/\epsilon_i} e^{(t/\delta-1)}) (1 - \delta e^{-x/\epsilon_i} e^{(t/\delta-1)}) , \\ R_l(x, t) &= 1 - \delta e^{-x/\epsilon_i} e^{(t/\delta-1)} , \end{aligned} \quad (28)$$

where the subscript l denotes the late time solution. The interface position is defined by $s(t) = v(t - t_2)$, so the above solutions hold for $x \in [s(t), L]$. This stage finishes when all soluble material in the column has been extracted, that is $R(L) = R_c$, where the corresponding time may be calculated from (28), $t_f = \delta(1 + L/\epsilon_i)$ ($t_f^* = \delta(1 + L/\epsilon_i)\tau$).

Once the radius is determined the void fraction $\epsilon(x, t)$ may be specified using equation (23) while the solvent velocity $u(x, t) = \epsilon_i/\epsilon(x, t)$.

The extracted fraction is defined as the ratio of material collected at the outlet to the total amount available. Since Stage 1 accounts for the period before solvent reaches the outlet $X = 0$ for $t \leq t_1$. Subsequently we may write

$$X_e(t) = \int_{t_1}^t c_e(L, \xi) d\xi \quad \text{for } t_1 \leq t \leq t_2, \quad (29)$$

$$X_l(t) = \int_{t_1}^{t_2} c_e(L, \xi) d\xi + \int_{t_2}^t c_l(L, \xi) d\xi \quad \text{for } t_2 \leq t \leq t_f. \quad (30)$$

This leads to

$$X_e(t) = (1 - E_L)(t - t_1) + \mathcal{O}(\delta^2), \quad \text{for } t_1 \leq t \leq t_2 \quad (31)$$

$$\begin{aligned} X_l(t) &= X_e(t_2) + t - t_2 - E_L t_2 (e^{(t/t_2-1)} - 1) + \mathcal{O}(\delta^2) \\ &= t - (1 - E_L)t_1 - E_L t_2 e^{(t/t_2-1)} + \mathcal{O}(\delta^2), \quad \text{for } t_2 \leq t \leq t_f, \end{aligned} \quad (32)$$

where $E_L = \exp(-L/\epsilon_i)$. Since we neglect terms of $\mathcal{O}(\delta^2)$ and $t_2 = \delta > t_1$ the quadratic terms arising from integrating t in the c_e equation have been omitted. In dimensional form these become

$$X_e^*(t^*) \approx \frac{\dot{m}^* c_s^*}{M_{tot}^* \rho_s^*} (1 - E_L)(t^* - t_1^*), \quad \text{for } t_1^* \leq t^* \leq t_2^*, \quad (33)$$

$$X_l^*(t^*) \approx \frac{\dot{m}^* c_s^*}{M_{tot}^* \rho_s^*} \left(t^* - (1 - E_L)t_1^* - E_L t_2^* \exp\left(\frac{t^*}{t_2^*} - 1\right) \right), \quad \text{for } t_2^* \leq t^* \leq t_2^* \left(1 + \frac{L^*}{\epsilon_i \mathcal{L}^*}\right), \quad (34)$$

where $E_L = \exp(-L^*/(\epsilon_i \mathcal{L}^*))$, $\mathcal{L}^* = R_i^* u_i^*/(2(1 - \epsilon_i)k_i^*)$, $t_1^* = L^*/u_i^*$, $t_2^* = (R_i^* - R_c^*)\rho_e^*/(k^* c_s^*)$, $\tau^* = \rho_e^* R_i^*/(k^* c_s^*)$ and we have used the definition $u_i^* = \dot{m}^*/(\epsilon_i \rho_s^* A_b^*)$.

In practical situations $E_L \ll 1$ (in the examples of the following sections the typical value is 10^{-3}) in which case for the majority of the process the extracted fraction rate $dX^*/dt^* \approx \dot{m}^* c_s^*/(M_{tot}^* \rho_s^*)$ is constant. Hence the extraction rate increases with an increase in the inlet mass flux and the fluid's saturation concentration or a decrease in the solvent density. These are the key factors affecting the rate, at least during the linear period (which lasts for a significant proportion of the process).

The above analytical solutions permit the verification of the outlet boundary condition. From (27) the early time concentration gradient at the inlet and outlet takes the form

$$\frac{\partial c_0}{\partial x}(0, t) = \frac{c_s^*}{\epsilon \mathcal{L}}(1 - t^*/\tau^*), \quad \frac{\partial c_0}{\partial x}(L, t) = \frac{c_s^* E_L}{\epsilon \mathcal{L}}(1 + t^*/\tau^* - 2t^* E_L/\tau^*). \quad (35)$$

That is $c_{0x^*}^*(L^*, t^*) = \mathcal{O}(E_L c_{0x^*}^*(0, t^*))$ which verifies the discussion behind the neglect of the diffusive term in the flux condition of (16).

The above solution involves the two unknowns c_s^*, k^* . Practically these may be determined by taking two experimental data points for the extracted fraction and then solving the two simultaneous equations numerically. Of course more data points could be used and an average taken. Using the above approximation to determine the unknown parameters is considerably simpler than solving the PDE system and then optimising the unknowns. The only contentious issue is that, without knowing the value of t_2^* (which depends on the unknowns) it is hard to say whether the data points fall into early or late time solutions. Consequently we would solve assuming the results lie in one region and then adjust if the points used were found to be outside of the resultant $t_2^* = \delta\tau$. The determination of parameter values is made significantly simpler through the observation that the extracted fraction has a linear form and hence constant slope for much of the process thus permitting c_s^* to be calculated from the slope. The value of k^* requires information from the nonlinear part of the process, that is for large times.

4.2. Model for two distinct solubilities

We now consider the situation where the solubility changes at a known value of the radius, denoted R_w . For $R \in [R_w, 1]$ the solubility is c_s , for $R \in [R_c, R_w]$ the solubility is denoted c_w . The early time behaviour is identical to Stages 1 and 2 of the single solubility model, but now Stage 2 ends when the inlet radius reaches R_w . Subsequently the region from the inlet to the point where $R = R_w$ has solubility c_w while the region ahead of this, with $R > R_w$, has solubility c_s .

There are various possible solution forms at this stage, depending on the solubility and relative thickness of the two layers. Below we will detail the case where the interface between the two solubility regions reaches the outlet before the inlet region reaches $R = R_c$. This is motivated by the example studied in §6, where the second solubility is much lower than the first and so we anticipate all material with c_s being removed before the c_w section is stripped at the inlet. An alternative scenario is that the inlet is stripped before the interface between the two solubilities reaches the outlet, then the model will require two moving fronts. The BIC model [7] would require R to decrease for the first stage but stay constant for the second (since material is being removed from inside intact cells). It is also possible that with the change in solubility there is a change in reaction rate, manifested through k . In all cases a similar analysis to that discussed below would provide the appropriate solution forms.

Now we summarise the results of Appendix A.2.

Stages 1 and 2. In these first stages all the material extracted has the solubility c_s . Therefore, the concentration and radius are identical to those of Stages 1 and 2 for the single solubility model, equations (27). In this case they hold until the solubility first changes, when $R(0, t_2) = R_w$. From equation (27) we determine the time when this stage ends as

$$t_2 = 1 - R_w. \quad (36)$$

Subsequently we again seek a travelling wave solution.

Stage 3. Now there is material to extract both before and after the front. To first order the concentration is

$$c_l(x, t) = \begin{cases} c_w & \text{if } x \leq s_1(t) \\ 1 - (1 - c_w) \left(1 + (1 - R_w) \left(1 - \exp\left(-\frac{x-s_1(t)}{\epsilon_i}\right) \right) \right) \exp\left(-\frac{x-s_1(t)}{\epsilon_i}\right) & \text{if } x \geq s_1(t) \end{cases} \quad (37)$$

For $x \leq s_1(t)$ the solution indicates that the concentration rapidly reaches its new, lower, saturation value c_w (this could be improved by seeking higher order terms or treating the boundary layer at the inlet). The error is greatest when $s_1 \approx 0$, in the Appendix it is explained that the error decreases exponentially away from the inlet. Using the values of §6 shows a maximum error of around 10% which will be negligible by the time the front reaches the outlet.

The radius is given by

$$R_l(x, t) = \begin{cases} R_w & \text{if } x \leq s_1(t) \\ 1 - (1 - R_w)e^{-(x-s_1(t))/\epsilon_i} & \text{if } x \geq s_1(t) \end{cases}, \quad (38)$$

and the front position

$$s_1(t) = \epsilon_i(1 - c_w) \frac{t - t_2}{1 - R_w} = \epsilon_i(1 - c_w) \left(\frac{t}{1 - R_w} - 1 \right). \quad (39)$$

The solution $R_l = R_w$ for $x \leq s_1$ is consistent with the concentration and subject to the same restrictions.

This solution holds until $t = t_3$ such that $s_1(t_3) = L$ where

$$t_3 = (1 - R_w) \left(1 + \frac{L}{\epsilon_i(1 - c_w)} \right). \quad (40)$$

As a check on the solutions we note that when $R_w = R_c$, $c_w = 0$ and the single solubility results are retrieved.

Stage 4. In this stage all c_s material has been removed and so again we have a single solubility problem. This is easily solved to determine

$$c_{f1}(x, t) \sim c_w(1 - e^{-x/\epsilon_i}), \quad R_{f1}(x, t) \sim R_w - c_w(t - t_3)e^{-x/\epsilon_i}. \quad (41)$$

Stage 4 ends when $R(0, t) = R_c$ at time

$$t_4 = t_3 + \frac{R_w - R_c}{c_w} = (1 - R_w) \left(1 + \frac{L}{\epsilon_i(1 - c_w)} \right) + \frac{R_w - R_c}{c_w}. \quad (42)$$

Stage 5. The final stage is simply a single solubility travelling wave and follows the method of Stage 3 from the previous section. Then, behind the wave $c = 0$, $R = R_c$, and in front the concentration and radius for $t_4 \leq t \leq t_f$ are now given by

$$c_{f2}(x, t) \sim c_w(1 - e^{-(x-s_2(t))/\epsilon_i}), \quad (43)$$

$$R_{f2}(x, t) \sim R_c + (R_w - R_c)(1 - e^{-(x-s_2(t))/\epsilon_i}), \quad (44)$$

where the front position is

$$s_2(t) = \frac{\epsilon_i c_w}{R_w - R_c} (t - t_4). \quad (45)$$

The process ends when $s_2(t_f) = L$, that is

$$t_f = t_4 + \frac{(R_w - R_c)L}{\epsilon_i c_w}. \quad (46)$$

Using the above expressions one can now obtain the extracted fraction for the two solubility model. As before we will neglect all terms of $\mathcal{O}(\delta^2)$. The previous single solubility result holds for $t_1 \leq t \leq t_2$ where $t_1 = L/u$, $t_2 = (1 - R_w)$,

$$X_e(t) = \int_{t_1}^t (1 - E_L)(1 - tE_L) dt = (1 - E_L)(t - t_1) + \mathcal{O}(\delta^2).$$

For $t_2 < t \leq t_3$ where $t_3 = (1 - R_w)(1 + L/(\epsilon_i(1 - c_w)))$,

$$\begin{aligned} X_l(t) &= (1 - E_L)(t_2 - t_1) + \int_{t_2}^t (1 - (1 - c_w)E_L e^{(1-c_w)(t-t_2)/(1-R_w)} + \mathcal{O}(\delta)) dt \\ &= t - t_1(1 - E_L) - (1 - R_w)E_L \exp\left((1 - c_w)\left(\frac{t}{1 - R_w} - 1\right)\right) + \mathcal{O}(\delta^2). \end{aligned}$$

For $t_3 < t \leq t_4$ where $t_4 = t_3 + (R_w - R_c)/c_w$,

$$X_{f1}(t) = X_l(t_3) + \int_{t_3}^t c_w(1 - E_L) + \mathcal{O}(\delta^2) = t_3 - t_2 + (1 - E_L)(c_w(t - t_3) - t_1) + \mathcal{O}(\delta^2).$$

Finally, for $t_4 < t \leq t_f$ where $t_f = t_4 + L(R_w - R_c)/(c_w \epsilon_i)$,

$$\begin{aligned} X_{f2}(t) &= X_{f1}(t_4) + \int_{t_4}^t c_w (1 - E_L e^{c_w(t-t_4)/(R_w-R_c)}) + \mathcal{O}(\delta^2) \\ &= t_3 - t_2 - (1 - E_L)t_1 + c_w(t - t_3) \\ &\quad - E_L(R_w - R_c) \exp\left(\frac{c_w(t - t_3)}{R_w - R_c} - 1\right) + \mathcal{O}(\delta^2). \end{aligned}$$

In dimensional form,

$$X_e^*(t^*) \approx \frac{\dot{m}^* c_s^*}{M_{tot}^* \rho_s^*} (1 - E_L) (t^* - t_1^*), \quad \text{for } t_1^* \leq t^* \leq t_2^*, \quad (47)$$

$$\begin{aligned} X_l^*(t^*) &\approx \frac{\dot{m}^* c_s^*}{M_{tot}^* \rho_s^*} \left(t^* - t_1^* (1 - E_L) \right. \\ &\quad \left. - t_2^* E_L \exp\left(\left(1 - \frac{c_w^*}{c_s^*}\right)\left(\frac{t^*}{t_2^*} - 1\right)\right) \right), \quad \text{for } t_2^* \leq t^* \leq t_3^*, \end{aligned} \quad (48)$$

$$X_{f1}^*(t^*) \approx \frac{\dot{m}^* c_s^*}{M_{tot}^* \rho_s^*} \left(t_3^* - t_2^* + (1 - E_L) \left(\frac{c_w^*}{c_s^*} (t^* - t_3^*) - t_1^* \right) \right), \quad \text{for } t_3^* \leq t^* \leq t_4^*, \quad (49)$$

$$\begin{aligned} X_{f2}^*(t^*) &\approx \frac{\dot{m}^* c_s^*}{M_{tot}^* \rho_s^*} \left(t_3^* - t_2^* - (1 - E_L) t_1^* + \frac{c_w^*}{c_s^*} (t^* - t_3^*) \right. \\ &\quad \left. - \tau^* E_L \frac{R_w^* - R_c^*}{R_i^*} \exp\left(\frac{c_w^* R_i^* (t^* - t_3^*)}{c_s^* \tau^* (R_w^* - R_c^*)} - 1\right) \right), \quad \text{for } t_4^* \leq t^* \leq t_f^*, \end{aligned} \quad (50)$$

where $E_L = \exp(-L^*/(\epsilon_i \mathcal{L}))$, $\mathcal{L} = R_i^* u_i^*/(2(1 - \epsilon_i)k_i^*)$, $t_1^* = L^*/u_i^*$, $t_2^* = \tau^*(1 - R_w^*/R_i^*)$, $t_3^* = \tau^*(1 - R_w^*/R_i^*)(1 + L^*/(\epsilon_i \mathcal{L}(1 - c_w^*/c_s^*)))$, $t_4^* = t_3^* + c_s^*(R_w^* - R_c^*)/(c_w^* R_i^*)$, $t_f^* = t_4^* + L^* c_s^*(R_w^* - R_c^*)/(c_w^* R_i^* \mathcal{L} \epsilon_i)$, $\tau^* = \rho_e^* R_i^*/(k^* c_s^*)$ and we have again used the definition $u_i^* = \dot{m}^*/(\epsilon_i \rho_s^* A_b^*)$.

Again we note the possibility of linear sections: the first part with gradient $\dot{m}^* c_s^*/(M_{tot}^* \rho_s^*)$ matches that of the single solubility model, the second has gradient $\dot{m}^* c_w^*/(M_{tot}^* \rho_s^*)$. These regions join where the exponential term of (48) becomes non-negligible. In general the double solubility model is clearly more complex than the single version. In the above example there are five distinct stages, and this is just for the option where all c_s material is removed before the c_w section is removed at the inlet. The physical situation may be such that instead of a change in solubility there is a change in the mass transfer coefficient or the radius is fixed after the shift in solubilities. Our choice was based on the example used in §6. A similar analysis should be possible for all other cases.

5. Numerical solution

In the previous section, we derived analytical solutions valid for small Da , Pe^{-1} and δ . In this section, we verify the accuracy of these solutions by comparing them to a numerical solution of the full model.

For the single solubility system the governing equations for the three stages of the process are the same, however the domain where they hold changes for each stage. These domains are $\Omega_1 = [0, l(t)]$, $\Omega_2 = [0, L]$ and $\Omega_3 = [s(t), L]$, for stages 1, 2 and 3, respectively, where $l(t) = t/Da$ and $s(t)$ is unknown which has to be found as part of the solution. This suggests a different numerical strategy for each stage. However, as we will show, stages 2 and 3 can be dealt with together using a similar approach to that previously employed for adsorption processes in porous media [27, 28].

Before presenting the numerical strategy we define the new variable $g = \epsilon c$ and rewrite equations (22) and (20) as

$$Da \frac{\partial g}{\partial t} + \epsilon_i \frac{\partial}{\partial x} \left[\frac{g}{1 - (1 - \epsilon_i)R^2} \right] = Pe^{-1} \frac{\partial^2 g}{\partial x^2} + R \left[1 - \frac{g}{1 - (1 - \epsilon_i)R^2} \right], \quad (51)$$

$$\frac{\partial R}{\partial t} = - \left[1 - \frac{g}{1 - (1 - \epsilon_i)R^2} \right], \quad (52)$$

subject to the boundary conditions

$$\epsilon_i \left[\frac{g}{1 - (1 - \epsilon_i)R^2} \right] \Big|_{x=0} - Pe^{-1} \frac{\partial g}{\partial x} \Big|_{x=0} = 0, \quad \frac{\partial}{\partial x} \left[\frac{g}{1 - (1 - \epsilon_i)R^2} \right] \Big|_{x=L} = 0. \quad (53)$$

We do not specify the initial conditions yet since they change at each stage.

Stage 1: Equations (51)-(52) hold in the spatial domain Ω_1 until the solvent reaches the end of the column at time $t_1 = LDa$. We use a popular strategy to tackle moving boundaries in numerical schemes that consists on mapping the variable domain into a fixed, unit domain using a Landau type transformation. In our case, the Landau transformation is $\xi = x/l(t)$, leading to the unknown functions $\tilde{g}(\xi, t) = g(x, t)$ and $\tilde{R}(\xi, t) = R(x, t)$. In terms of the transformed

variables, the governing equations (51)-(52) read

$$\frac{\partial \tilde{g}}{\partial t} - \frac{\dot{l} \xi}{l \text{Da}} \frac{\partial \tilde{g}}{\partial \xi} + \frac{\epsilon_i}{l \text{Da}} \frac{\partial}{\partial \xi} \left[\frac{\tilde{g}}{1 - (1 - \epsilon_i) \tilde{R}^2} \right] = \frac{\text{Pe}^{-1}}{\text{Da} l^2} \frac{\partial^2 \tilde{g}}{\partial \xi^2} + \frac{\tilde{R}}{\text{Da}} \left[1 - \frac{\tilde{g}}{1 - (1 - \epsilon_i) \tilde{R}^2} \right], \quad (54)$$

$$\frac{\partial \tilde{R}}{\partial t} - \frac{\dot{l} \xi}{l} \frac{\partial \tilde{R}}{\partial \xi} = - \left[1 - \frac{\tilde{g}}{1 - (1 - \epsilon_i) \tilde{R}^2} \right]. \quad (55)$$

Note the only true unknowns in (54)-(55) are \tilde{g} and \tilde{R} , since the position of the moving boundary, $l(t) = \text{Da}^{-1}t$, and its derivative, $\dot{l} = \text{Da}^{-1}$, are known. The boundary conditions (53) become

$$\epsilon_i \left[\frac{\tilde{g}}{1 - (1 - \epsilon_i) \tilde{R}^2} \right] \Big|_{\xi=0} - \frac{\text{Pe}^{-1}}{l} \frac{\partial \tilde{g}}{\partial \xi} \Big|_{\xi=0} = 0, \quad \frac{1}{l} \frac{\partial}{\partial \xi} \left[\frac{\tilde{g}}{1 - (1 - \epsilon_i) \tilde{R}^2} \right] \Big|_{\xi=1} = 0. \quad (56)$$

Initially $l(0) = 0$, so the domain has zero thickness, and there are no initial conditions. To overcome this issue, we simply initialise the code with $l(t_0) = l_0$, where t_0 is very small and $l_0 = \text{Da}^{-1}t_0$, and apply $\tilde{g}(\xi, t_0) = 0$ and $\tilde{R}(\xi, t_0) = 1$.

To solve (54)-(56), we implement an explicit finite difference scheme with suitable upwind discretisation for first-order spatial derivatives and central differences for the diffusion term. So, the time derivatives in the governing equations are approximated via

$$\frac{\partial \tilde{g}}{\partial t} \approx \frac{\tilde{g}_i^{n+1} - \tilde{g}_i^n}{\Delta t}, \quad \frac{\partial \tilde{R}}{\partial t} \approx \frac{\tilde{R}_i^{n+1} - \tilde{R}_i^n}{\Delta t} \quad (57)$$

and spatial derivatives via

$$\frac{\partial \tilde{g}}{\partial \xi} \approx \frac{\tilde{g}_{i+1}^n - \tilde{g}_i^n}{\Delta \xi}, \quad \frac{\partial \tilde{R}}{\partial \xi} \approx \frac{\tilde{R}_{i+1}^n - \tilde{R}_i^n}{\Delta \xi}, \quad \frac{\partial f}{\partial \xi} \approx \frac{f_i^n - f_{i-1}^n}{\Delta \xi}, \quad \frac{\partial^2 \tilde{g}}{\partial \xi^2} \approx \frac{\tilde{g}_{i+1}^n - 2\tilde{g}_i^n + \tilde{g}_{i-1}^n}{\Delta \xi^2}, \quad (58)$$

where $f = g/(1 - (1 - \epsilon_i)R^2)$. We ensure that all the stability conditions are satisfied.

Stages 2 and 3: For a compact formulation that allows Stages 2 and 3 to be tackled together, we rewrite (51)-(52) using the the Heaviside function $H(R - R_c)$ as

$$\text{Da} \frac{\partial g}{\partial t} + \epsilon_i \frac{\partial}{\partial x} \left[\frac{g}{1 - (1 - \epsilon_i)R^2} \right] = \text{Pe}^{-1} \frac{\partial^2 g}{\partial x^2} + R \left[1 - \frac{g}{1 - (1 - \epsilon_i)R^2} \right] H(R - R_c), \quad (59)$$

$$\frac{\partial R}{\partial t} = - \left[1 - \frac{g}{1 - (1 - \epsilon_i)R^2} \right] H(R - R_c), \quad (60)$$

where $H(R - R_c)$ disables the source term in (59) and (60) altogether wherever $R - R_c = 0$. These equations are subject to the boundary conditions (53). The initial conditions are

$$R(x, t_1) = R_{s1}(x), \quad g(x, t_1) = g_{s1}(x), \quad (61)$$

where $R_{s1}(x)$ and $g_{s1}(x)$ are the profiles at the end of Stage 1, $t = t_1$. An explicit scheme for (59)-(61) is used in an analogous way to Stage 1, i.e., using an upwind discretisation for the advection term, central differences for the diffusion term, and ensuring that all stability conditions are satisfied.

5.1. Extension to two solubilities

The switch between solubilities does not involve a particular challenge for the numerical scheme. Using the function $\chi = \chi(R)$ that switches from 1 to c_ω when $R = R_\omega$ (see Appendix A) the system (59)-(60) becomes

$$\text{Da} \frac{\partial g}{\partial t} + \epsilon_i \frac{\partial}{\partial x} \left[\frac{g}{1 - (1 - \epsilon_i)R^2} \right] = \text{Pe}^{-1} \frac{\partial^2 g}{\partial x^2} + R \left[\chi - \frac{g}{1 - (1 - \epsilon_i)R^2} \right] H(R - R_c), \quad (62)$$

$$\frac{\partial R}{\partial t} = - \left[\chi - \frac{g}{1 - (1 - \epsilon_i)R^2} \right] H(R - R_c), \quad (63)$$

and we may proceed as before.

5.2. Comparison between numerics and perturbation

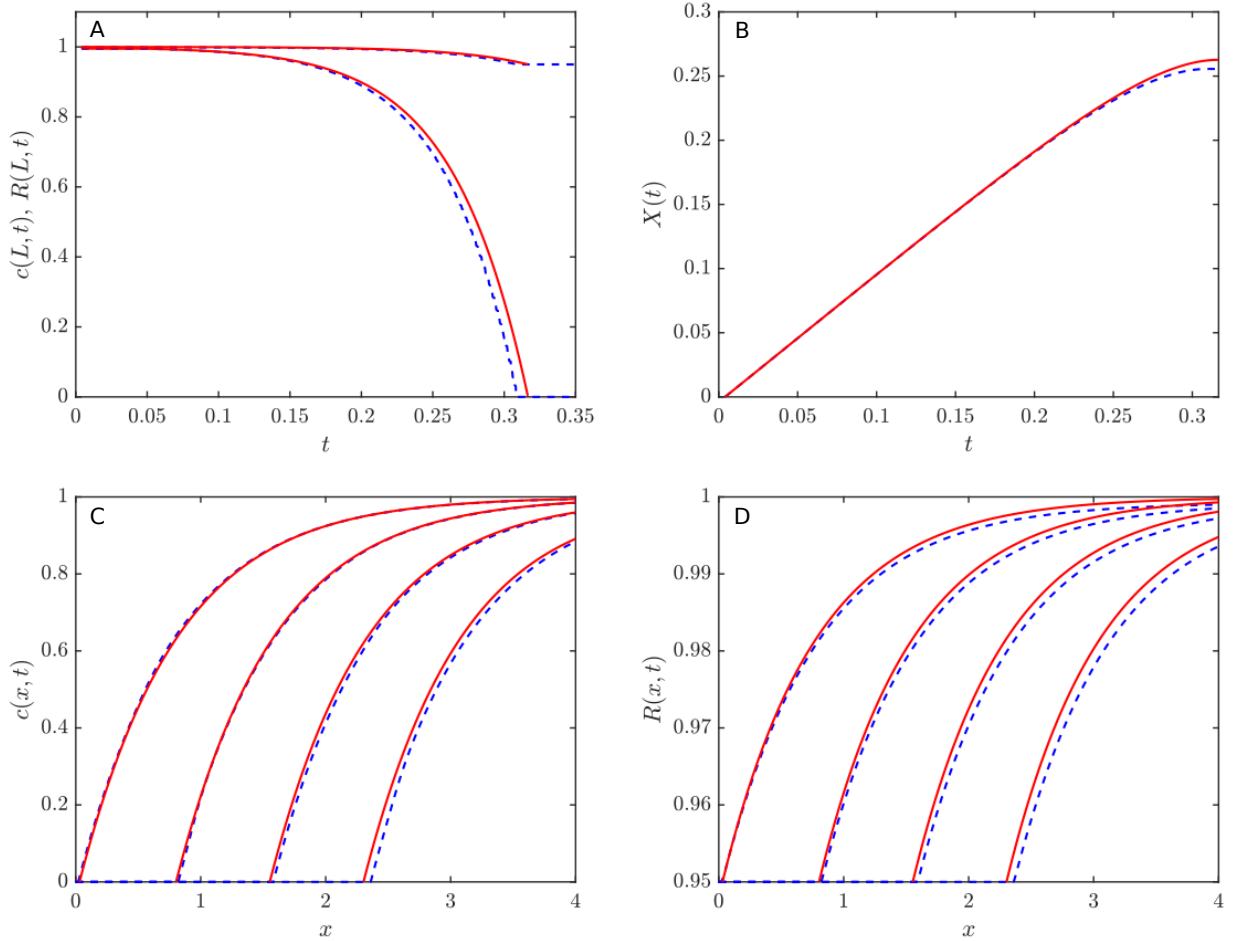


Figure 3: Numerical (dashed) and perturbation (solid) solutions using $L = 4$, $\text{Da} = \text{Pe}^{-1} = 0.001$, $R_c = 0.95$, $\epsilon_i = 0.75$. Panel A shows the outlet concentration and radius, $c(L,t), R(L,t)$. The concentration profile in panel C and radius in Panel D correspond (from left to right) to times $t = 0.05, 0.1, 0.15, 0.2$.

In Figure 3 we compare the predictions of the numerical solution (dashed line) with that of the perturbation (solid line) at various positions and times, with $\text{Da} = \text{Pe}^{-1} = 0.001$, $\epsilon = 0.75$

and $R_c = 0.95$. Figure 3A shows the variation of c, R at the outlet. For early times the fluid is saturated with material and $c(L, t) \approx 1$. This lasts until around $t \approx 0.06$ when c starts to decrease monotonically until it reaches zero at $t \approx 0.32$. Since the saturated fluid cannot remove material $R \approx 1$ until the concentration begins to decrease after which it slowly decays to the core value $R_c = 0.95$. The numerical and perturbation solutions are clearly close, with only slight differences visible at the end of the process.

Figure 3B shows the variation of $X(t)$. The perturbation and numerical solutions are virtually indistinguishable except at the very end. Recalling the discussion of an approximately linear section in §4 for small E_L here we note that $E_L = \exp(-L/\epsilon_i) = \exp(-4/0.75) \approx 0.005$. According to equations (31, 32) the linear section of the curve is well approximated by $X(t) \approx t - t_1$, the exponential component only becoming noticeable in the final stages.

The concentration and radius at times $t = 0.05, 0.1, 0.15, 0.2$ are shown in Figures 3C,D. The self-similar form is evident and the numerical solution closely follows the travelling wave form of the perturbation. It may be noted that at the exit $x = L = 4$ the concentration gradient appears to be non-zero, contradicting the applied boundary condition $c_x(L, t) = 0$. This is due to the presence of a very narrow boundary layer of thickness $\mathcal{O}(\sqrt{Pe^{-1}})$. With the chosen value $Pe^{-1} = 0.001$ the resultant boundary layer has thickness of order $\mathcal{O}(0.03)$ which is hard to distinguish on the above graph. However, we have verified its existence in separate calculations using a much finer grid.

Figure 4 shows a similar set of results but now $R_c = 0.9$. The same general behaviour may be observed but with slightly larger differences between the two sets of curves. This is to be expected: the perturbation is based on the small parameter $\delta = 1 - R_c$. As R_c decreases δ increases and hence so does the error. However, again the two solutions for X are indistinguishable until the final stages and have an approximately linear form for a large amount of the process. Separate numerical calculations have confirmed the existence of a boundary layer over which the concentration gradient tends to zero.

The main difference between numerics and perturbation in panels C and D in Figures 3, 4 is really the point where the curve begins: the numerical solution is slightly ahead. In Figure 5 we compare the position of the front $s(t)$ for the two cases. The perturbation is always slightly behind, indicating a slightly slower velocity. This could be improved by taking higher order terms but may be complicated by the contribution of $Da/\delta, Pe^{-1}$ terms which may enter into lower order expressions. As time increases the small difference in speeds then acts to move the curves farther apart. However, even at the end of the process, for the case shown in Figure 5B the error is below 5%. So we may conclude the perturbation solution is, in general, highly accurate. Further, since the extracted fraction is the quantity of main interest the very close correspondence between curves suggests that the perturbation is particularly accurate for tracking this quantity. Consequently in the following section, where we examine the removal of lanolin from woollen fibres, we will focus primarily on the perturbation solution since this gives a clear picture of the role of the system parameters.

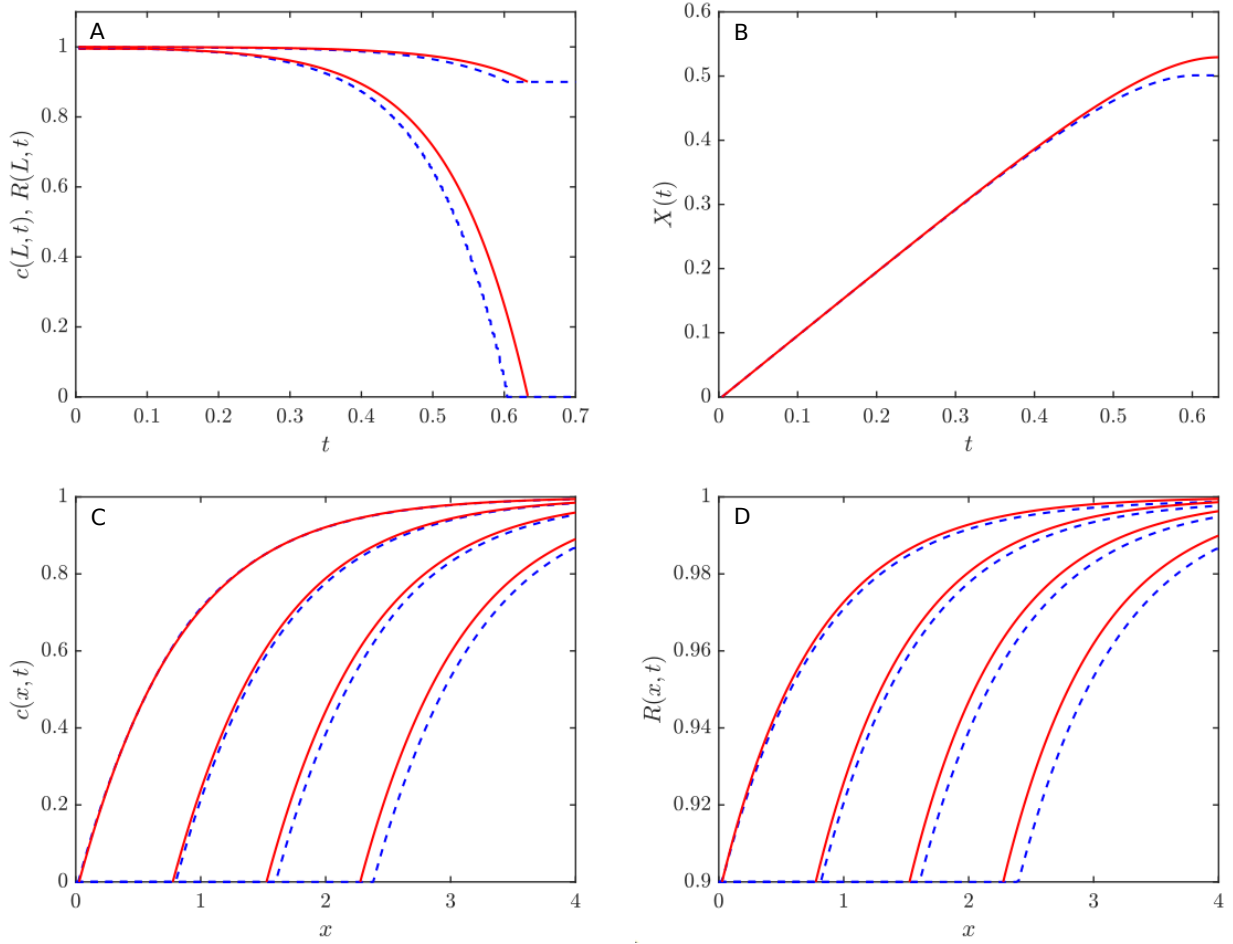


Figure 4: Numerical (dashed) and perturbation (solid) solutions using $L = 4$, $\text{Da} = \text{Pe}^{-1} = 0.001$, $R_c = 0.9$, $\epsilon_i = 0.75$. The profiles in panels C, D correspond (from left to right) to times $t = 0.1, 0.2, 0.3, 0.4$.

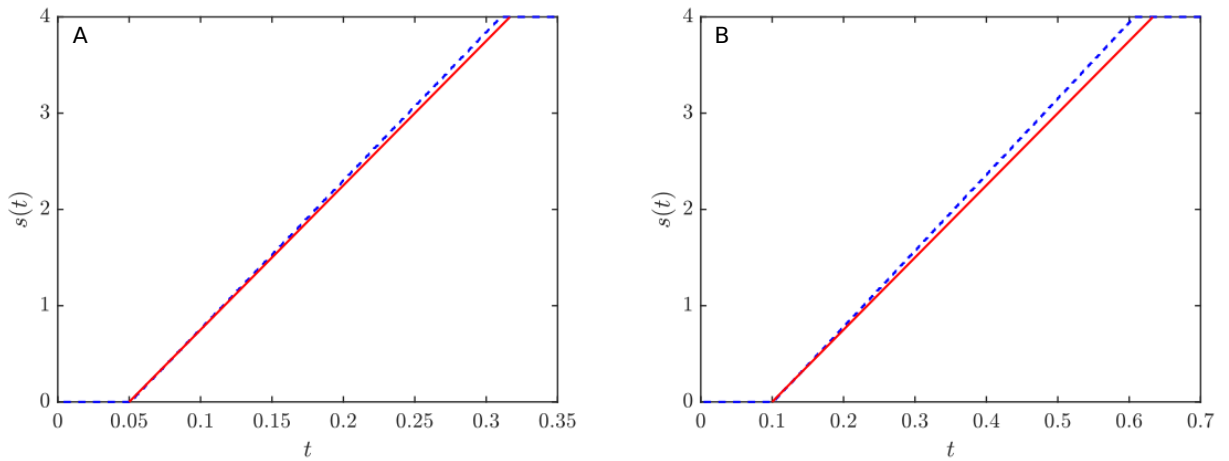


Figure 5: Evolution of the moving boundary $s(t)$ from the numerical and perturbation solutions for $L = 4$, $\text{Da} = \text{Pe}^{-1} = 0.001$, $\epsilon_i = 0.75$ and (A) $R_c = 0.95$, (B) $R_c = 0.9$.

6. Application to lanolin removal from wool fibres

In this section we apply the above model to the removal of lanolin from wool fibres. For this we take the operating conditions and data from the experiments described in [29].

Table 2: Experimental operating conditions of [29].

Temperature	30 °C
Pressure	70, 120, 150 bar
Solvent mass flowrate, \dot{m}^*	3, 4, 5 kg/h
\dot{m}^* (in SI units)	$8.33, 11.11, 13.89 \times 10^{-4}$ kg/s
Wool packing density, ρ_B^*	127, 159, 227, 318 kg/m ³
Solvent composition, % wt.	95% CO ₂ – 5% ethanol

Table 3: Parameter values from the experiments of [29]

Property	Sym.	Units	Value				Ref./Method
Extractor vessel and wool load							
Inner rad.	R_b^*	m	0.015				[29]
Section	A_b^*	m ²	7.0686×10^{-4}				
Wool load	m_p^*	kg	0.013				
Wool dens.	ρ_p^*	kg/m ³	1314				[30] & [31]
Bulk dens.	ρ_B^*	kg/m ³	127	159	227	318	[29]
Volume	V_b^*	m ³	1.0×10^{-4}	8.2×10^{-5}	5.7×10^{-5}	4.1×10^{-5}	$V_b^* = m_p^*/\rho_B$
Length	L^*	m	0.145	0.116	0.081	0.058	$L^* = V_b^*/A_b^*$
Porosity	ϵ_i	–	0.903	0.879	0.827	0.758	$\epsilon_i = 1 - \rho_B^*/\rho_p^*$
Wool fibres and lanolin							
Initial rad.	R_i^*	m	10^{-5}				[29]
% wt. lan.	%lan		9.6%				Estimated from [29]
Layer rad.	R_w^*	m	9.52×10^{-6}				
Core rad.	R_c^*	m	9.25×10^{-6}				
Density	ρ_e^*	kg/m ³	940				Aspen Plus v9
Solvent							
Density	ρ_s^*	kg/m ³	783.3				Aspen Plus v9
Critical T	T_{crit}^*	K	310.55				
Critical P	P_{crit}^*	Pa	7.73×10^6				
Viscosity	μ^*	Pas	6.48×10^{-5}				Aspen Plus v9 with [32] ¹

¹Fields et al. [32] show that at 37 °C, the viscosity of the mixture 95% CO₂:5% ethanol doesn't change significantly with pressure. In their work, the viscosity of the solvent at 10^7 Pa is 6.35×10^{-5} Pas.

In Table 2 we present the operating conditions, in Table 3 we present the appropriate parameter values. The extractor vessel was a stainless steel AISI 316L Separex SCF 200.

According to [29] the initial wool load consisted of 60-65% wool fibres, 10-15% wax (lanolin) and proteins, 10% soluble stains (salts), 1-20% soil and vegetable matter (since the total amount with 1% of soil and vegetable matter does not reach 100%, we assume this is an error and should read 10%). The key parameters not provided in the Tables are the mass transfer coefficient k^* and the saturation concentrations c_s^*, c_w^* which are *a priori* unknown. They vary with the operating conditions and may be determined through comparison with experimental data. However, to determine the order of magnitude of various non-dimensional terms we note that in [19] for the experiments at 120 bar, the values given are $k^* = 4.1 \times 10^{-6} \text{s}^{-1}$ and $c_s^* \approx 0.632 \text{kg/m}^3$ (the value actually quoted is 0.807 g/kg solvent, multiplying by the solvent density ρ_s and converting to kilograms we obtain $c_s^* = 0.807 \times 10^{-3} \times 783.3 = 0.632 \text{kg/m}^3$). To estimate the diffusion coefficient we refer to [33, Fig. 5], this shows that for a supercritical liquid the inverse Bodenstein number $D_i^*/(2u^*R^*) \approx 2$ is approximately constant for Reynold's numbers $\text{Re} \in [0.1, 20]$ (note we have converted their definition from superficial velocity and particle diameter). This indicates that $D_i^* \approx 4u^*R^* = 4\epsilon_i u_i^* R^*/\epsilon$ varies with ϵ and R^* . Using the average of the mass flow rates from Table 2, $\dot{m}^* \approx 1.1 \times 10^{-3} \text{kg/s}$, and the average void fraction $\epsilon_i = 0.83$ of Table 3 we obtain a representative initial interstitial velocity

$$u_i^* = \frac{\dot{m}^*}{\epsilon_i \rho_s^* \pi R_b^{*2}} = 0.0024 \text{m/s}. \quad (64)$$

With a fibre radius $R^* = 10 \mu\text{m}$ we find $D_i^* = 9.6 \times 10^{-8} \text{m}^2/\text{s}$. We may now also calculate typical length- and time-scales of the extraction process

$$\mathcal{L}^* = \frac{R_i^* u_i^*}{2(1 - \epsilon_i) k^*} \approx 0.017 \text{m}, \quad \tau^* = \frac{\rho_e^* R_i^*}{k^* c_s^*} \approx 3753 \text{s}. \quad (65)$$

These indicate that the width of the main extraction zone is of the order 2cm while the time-scale for the process is of the order of one hour. The non-dimensional parameters may now be evaluated

$$\text{Da} = \frac{\mathcal{L}^*}{u_i^* \tau^*} \approx 0.002, \quad \text{Pe}^{-1} = \frac{4R_i^*}{\mathcal{L}^*} \approx 0.002, \quad \delta = 0.075. \quad (66)$$

In terms of the perturbation solution we note that the error incurred by neglecting $\text{Da}, \text{Pe}^{-1}$ will then be of order 0.2%, so justifying their omission from the respective equations. However, in the analysis we actually rescale time with δ , meaning that the time derivative term is of order $\text{Da}/\delta = 0.002/0.075 = 0.03$. So it is still valid to neglect the time derivative, even with this re-scaled time variable, but now the associated errors are of order 3%.

The exponential coefficient $E_L = \exp(-L^*/(\epsilon_i \mathcal{L}^*)) \sim \exp(-0.1/(0.83 \times 0.017)) \approx 10^{-3}$ is smaller than neglected terms and so has very little influence on the results.

6.1. Results and discussion

To determine the unknown parameter values we take the experimental data of [29] and carry out an optimisation procedure. The experiments indicate a clear change in solubility, see the discussion in [19], consequently we seek three unknowns k^*, c_s^*, c_w^* . Since c_s^* and c_w^* are thermodynamic properties, it is sensible to consider them as only dependent on temperature and pressure. Since the experiments are isothermal we anticipate a unique c_s^* and c_w^* for each pressure. The mass transfer coefficient, k^* , clearly depends on the flow (the force of which

depends, for example, on the fluid velocity and also its path through the material) and so will vary throughout the experiments. Consequently this is calculated for each data set. We employ nine data sets from [29] which involve three different pressures, leading to a total of fifteen parameters to optimize, i.e. nine mass transfer coefficients, three first fraction and three second fraction solubilities. In order to start our procedure initial guesses are required. Approximate values of the first two were discussed earlier, the final unknown c_w^* we take as some fraction of c_s^* (in practice we set $c_w^* = c_s^*/10$). The optimisation procedure employs an interior-point algorithm, using the MATLAB package *GlobalSearch* combined with the local solver *fmincon*, in order to reach a global constrained optimum. The objective function takes the form of the sum of the absolute value of the errors,

$$f = \sum_{i=1}^n |X_i^{*exp} - X_i^*|, \quad (67)$$

where X_i^* comes from the perturbation solution and X_i^{*exp} are the values provided by [29].

For the two solubility problem X_i^* has four components defined by equations (47 - 50). The switch between each stage depends on the value of the unknowns, consequently initially the whole X curve is calculated based on the estimated values and the objective function is then evaluated. The optimization algorithm is applied and new values for the parameters are calculated. These are used to recalculate the switching times and the process repeated until convergence is achieved. In order to compare model predictions with the single solubility model we carry out the procedure a second time but using only two unknowns k^* , c_s^* .

In Figure 6 we present a comparison of results from the single and double solubility perturbation solutions and the experimental data of [29] for the extracted fraction at various pressure, flow rate and wool packing conditions. Circles represent the data points, solid lines the two solubility model and dashed lines the single solubility model. In general the agreement between experiment and the two solubility model is excellent. However there are two rather prominent points where the agreement is clearly not so good, these are the first data points of the $P = 120$ bar, 3 kg/h, 127 kg/m³ and 4 kg/h, 159 kg/m³ graphs. In both cases the graphs only have four data points and only a single data point within the first linear stage. Consequently we may assume that in these cases there is not sufficient early time data to accurately characterise the behaviour. The single solubility model is clearly nowhere near as accurate, it suffers from the attempt to fit all data points. The inability to match the data confirms the observation of previous studies that lanolin removal occurs in two stages. The single solubility model could easily be adjusted to match just the early data points, where it is valid.

In §4 we discussed the linear forms of the extraction curve. This is apparent in the figures: the two solubility model clearly shows two linear sections while the one solubility case has a single linear section. Given the approximately linear behaviour for early times in both cases it is a simple matter to calculate c_s^* from the formula $X^* \approx \dot{m}^* c_s^* (t^* - t_1^*) / (M_{tot}^* \rho_s^*)$ (i.e. the gradient is $\dot{m}^* c_s^* / (M_{tot}^* \rho_s^*)$). This could be achieved using only the first data point for X^* or more early data points (if available) and then averaging. Similarly we could estimate c_w^* through the gradient of the second linear stage $\dot{m}^* c_w^* / (M_{tot}^* \rho_s^*)$.

The early time solutions for X_e^* , (equations (33) and (47)), show a linear variation with time and exhibit only a very weak dependence on k^* (through the value of E_L , which is of order 10^{-3}). Consequently, the early time solution, which in Fig. 6 lasts for almost half of the process time, indicates that X^* is independent of k^* with a high degree of accuracy. This

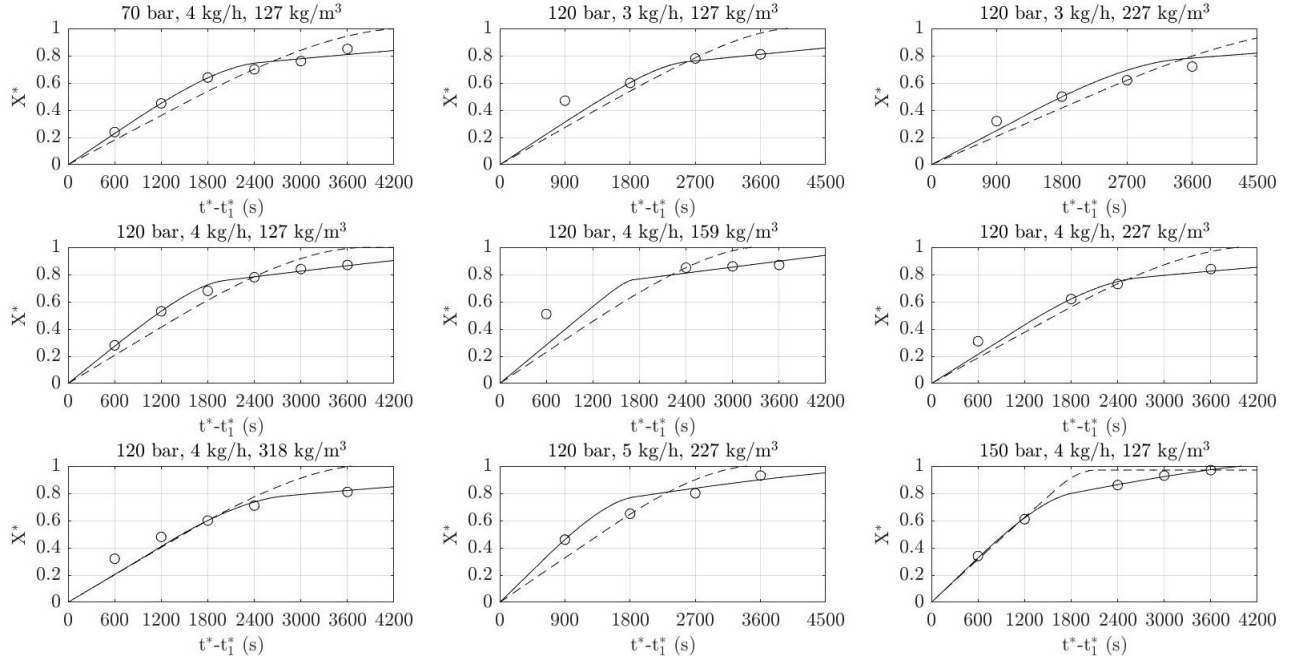


Figure 6: Extracted fraction curves obtained after optimizing the parameters k^* , c_s^* and c_w^* , using the perturbation method. The solid line represents the two solubility model, the dashed line the single solubility model and circles correspond to experimental data points.

phase corresponds to the period when the exit concentration $c^* \approx c_s^*$ (with errors of the order E_L , i.e. approximately 0.1%). The second linear stage also reveals little information about k^* . This also corresponds to a saturated outlet fluid but this time corresponding to the saturation value of the second layer, i.e. $c^* \approx c_w^*$. The value of k^* can therefore only be determined reliably through knowledge of the transition zone between the two linear sections or the very late time data (beyond the second linear section). The physical interpretation is that if the fluid is saturated at the outlet then the outlet measurements of the extracted fraction alone cannot be used to determine the mass transfer rate. The fluid could have been saturated close to the inlet or just before the outlet, there is no reliable way to distinguish between the two if the only data is values of X^* .

The parameter values for k^* , c_s^* and c_w^* , obtained through the optimisation of the two solubility model are presented in Table 4. The value of c_s^* obtained from the formula

$$c_s^* \approx M_{tot}^* \rho_s^* X^* / (\dot{m}^* (t^* - t_1^*)) , \quad (68)$$

using only the first data point is also given and labelled " c_s^* 1st point". Overall the agreement between the two c_s^* values is good, suggesting that using just the first data point is sufficient to provide a rough estimate of the value for the solubility (provided that point occurs within the first stage). Examination of the " c_s^* 1st point" row corresponding to $P = 120$ bar indicates that the majority of values are close to 0.45 kg/m^3 . The exceptions are the two cases mentioned earlier, for 3 kg/h , 127 kg/m^3 and 4 kg/h , 159 kg/m^3 , which have only a single data point within the linear region. Ignoring these two cases the remaining values show a maximum of around +11%/-13% deviation from 0.45. The range of k^* values in the table, $[0.83, 2.47] \times 10^{-6} \text{ m/s}$, are consistent with those of Figure 12 of Puiggené et al. [34] and also the low Reynolds number correlation reported by Tan et al. [35] for solid-SCF systems. They are close to those reported

by Valverde et al. [19] (although they use a slightly less accurate value for R_c^*).

Table 4: Value of the parameters obtained from optimization procedure for extraction at 30 °C and diverse pressure, mass flow rate and packing density conditions.

P (bar)	70	120							150
\dot{m}^* (kg/hr)	4	3		4				5	4
ρ_B^* (kg/m ³)	127	127	227	127	159	227	318	227	127
k^* ($\times 10^{-6}$) (m/s)	1.63	2.30	0.83	2.47	0.92	1.01	0.92	1.88	1.67
c_s^* 1 st pt (kg/m ³)	0.38	0.66	0.45	0.44	0.80	0.49	0.50	0.39	0.54
c_s^* (kg/m ³)	0.40	0.45							0.57
c_w^* (kg/m ³)	0.056	0.069							0.116

Physically we expect the value of k^* to increase with an increase in flow rate, \dot{m}^* (due to the increase in the force of the liquid on the solid). It could also be expected to vary with the bulk density but in a less obvious way. (The bulk density affects the void fraction ϵ_i which in turn affects the interstitial velocity, a low ρ_B^* indicates low $u^* \sim 1/\epsilon_i$. However k^* appears in the switching times and also $E_L = \exp(-L^*/(\epsilon_i \mathcal{L}^*))$. This combination suggests a nonlinear response). A nonlinear dependence is consistent with the results of [29, Fig. 7] who report a maximum mass transfer rate at around $\rho_B^* = 100$ kg/m³.

The influence of operating conditions on k^* , c_s^* and c_w^* is shown in Fig. 7. The first figure shows the variation of k^* with \dot{m}^* for fixed pressure and flow rate. As anticipated the value increases with increasing mass flow rate. When plotted against packing density, a monotonic decrease is observed. This behaviour is consistent with the [29, Fig. 7] who report a maximum k^* at $\rho_B^* > 100$ kg/m³ k^* followed by a monotonic decrease. Our results show no clear dependency of k^* on pressure, so we omit this figure (but note Valverde et al. [19] report a decrease of the mass transfer parameter with increasing pressure). Eychenne et al. [29] reported a yield increase with increasing pressure, but since solubility increases with pressure, it is difficult to determine the evolution of k^* based on this set of experimental results.

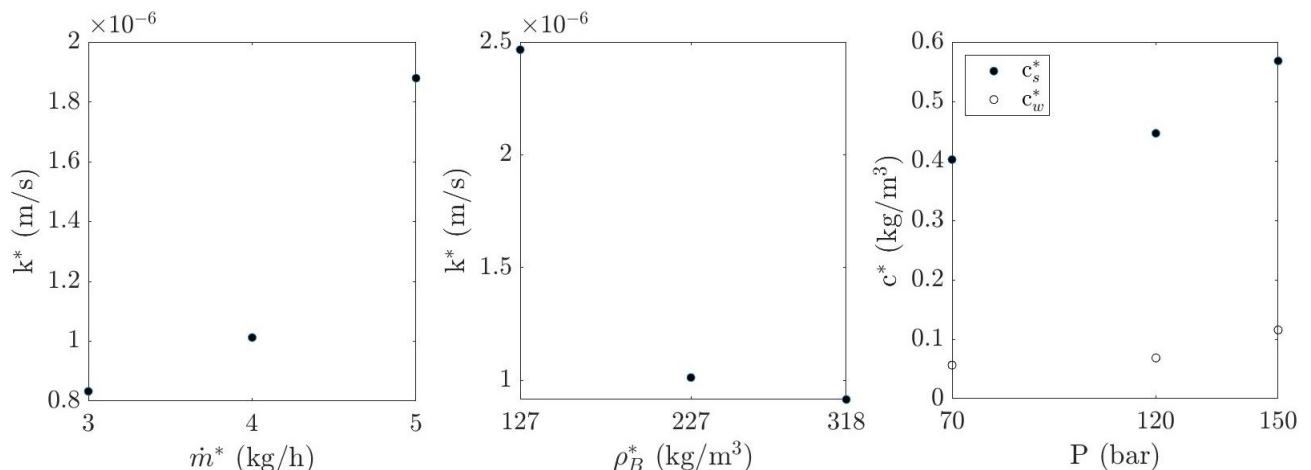


Figure 7: Dependence of k^* , c_s^* and c_w^* on diverse operating conditions at 30 °C. From left to right: k^* versus \dot{m}^* at 120 bar and 227 kg/m³; k^* versus ρ_B^* at 120 bar and 4 kg/h; c_s^* (solid points) and c_w^* (void points) versus pressure.

Finally, the remaining plot in Figure 7 shows the evolution of the two solubilities with pressure. Both fraction solubilities show a clear increase with increasing pressure, although it is more pronounced for c_s^* . This result is consistent with those of [29], which suggest a significant increase of the solubility between 120 and 150 bar. Note that the anomalous values obtained in Table 4 at 120 bar, 4 kg/h and 159 kg/m³ are excluded from the graphs. .

Figure 8 demonstrates how the outlet concentration and radius evolve according to the perturbation solutions, using the parameter values obtained through the optimisation. The single solubility model is shown as the dashed line. The initial value of the outlet concentration is zero until time t_1^* , when it suddenly jumps up. Since t_1^* is a lot less than the process time it is difficult to see. This is followed by a period of very slow decrease between t_1^* , t_2^* , from (27) it may be observed that the gradient is proportional to E_L . There is a slight mismatch between the solutions at t_2^* (a consequence of neglecting the time derivative which, as discussed, can lead to errors of the order 3%) this is followed by a rapid, nonlinear decrease to zero, where all material has been extracted after around 4000s. The two solubility model has similar qualitative features, a rapid jump followed by (a much shorter) linear decrease, a slight mismatch in solutions and then two stages of nonlinear decrease. The second nonlinear stage shows a very slow decrease due to the low value of $c_w^* < c_s^*$. The process ends at around 10800s. In the second figure, for the one solubility model, after time t_1^* the radius decreases monotonically to the final value of $R_c^* = 9.25\mu\text{m}$. With the two solubility model the radius at first decreases more rapidly followed by a slow decay to the final value.

7. Conclusions

In this paper we have developed a novel, mathematically consistent one-dimensional model for the slow extraction of material from a porous matrix by a flowing fluid. We have also developed the first approximate analytical solution for this process. The analysis leads to expressions for the concentration and radius throughout the column. Integrating the expression for the outlet concentration provides an expression for the variation of extracted fraction with time. This is an important quantity since one of the main goals in the field is to efficiently extract material, also this is what is typically measured during experiments.

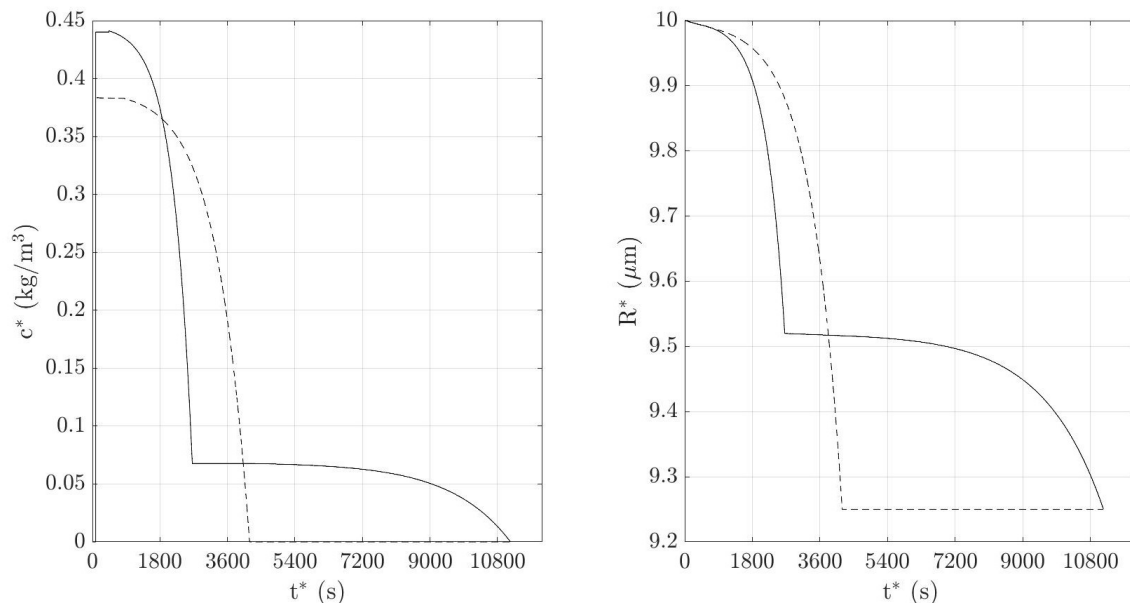


Figure 8: Concentration and radius profiles obtained from the perturbation method at 120 bar, 3 kg/h and 127 kg/m³. The solid line represents the two solubility model, the dashed line is the single solubility model.

The beauty of analytical solutions is that they clearly demonstrate the dependence upon the operating conditions, thus indicating how to optimise the extraction process. The dependence is not apparent with a purely numerical study. Here we found that for a significant portion of the process the extracted fraction exhibits very simple behaviour, varying linearly with mass flow rate and the saturation solubility and decreasing linearly with the solvent density. In the final stages the response is nonlinear, involving a more complex dependence on operational parameters.

The key model unknowns are the saturation solubility (or solubilities) and the mass transfer coefficient. In the case of a single solubility material the solubility is easily determined through matching the early data points for the extracted fraction with the analytical solution. In our model ‘early’ corresponds to an extended period where the outlet fluid is approximately saturated. The solution clearly shows that during the linear stage *it is not possible to accurately calculate the mass transfer coefficient*. The mass transfer coefficient may only be estimated through later data, when the outlet concentration starts to decrease. Consequently, in order to characterise an experiment it is important to have both early time data points to accurately determine the solubility as well as late data points, where the fluid is no longer saturated, to determine the mass transfer coefficient.

To validate the analytical solution comparison was made against a numerical solution. Subsequently the model was compared with experimental data for the extracted fraction of lanolin by a supercritical fluid. It has previously been established that the solubility of lanolin switches during the process, which required an extension of the solution to deal with a two solubility material. The analytical solution in this case involved three unknowns, the two solubilities and the mass transfer coefficient. The analysis was tailored for the specific case of lanolin removal, where the first stages involve a single solubility followed by a period when the inlet region has been stripped to reveal the next layer, which is significantly more difficult to remove. During

the initial stage, where the outer layer is being eroded, the model is identical to the single solubility case. The two solubility model exhibited two clear linear regions, the first with gradient proportional to the first solubility while the second is proportional to the second solubility. This provides a way to quickly estimate both quantities. However, the solutions show that the mass transfer coefficient may only be reliably calculated using data from the transition between the two linear regions or very late time data beyond the second linear period. This information is essential when interpreting experimental data.

There exist other possible scenarios involving, for example, a second layer with a lower solubility, a change in mass transfer rate or a constant radius. All of these could occur in different extraction processes. Since they were not relevant to the present study we did not consider all possible cases but they could be analysed using the methodology presented here and could form the basis of a future study.

Author Statement

The work has not been published previously and it is not under consideration for publication elsewhere. Its publication is approved by all authors. If accepted, it will not be published elsewhere in the same form, in English or in any other language, including electronically without the written consent of the copyright-holder.

Acknowledgements

T. Myers, F. Font and M. Aguares acknowledge the support grant No. PID2020-115023RB-I00 financed by MCIN/AEI/10.13039/501100011033/ and by “ERDF A way of making Europe”. M. Aguares also acknowledges grant no. MTM2017-84214-C2-2-P. F. Font acknowledges financial support from the Juan de la Cierva programme (grant IJC2018-038463-I). F. Font and T.G. Myers thank the CERCA Programme of the Generalitat de Catalunya, their work was also supported by the Spanish State Research Agency, through the Severo Ochoa and Maria de Maeztu Program for Centers and Units of Excellence in R&D (CEX2020-001084-M). F. Font is a Serra Hünter Fellow.

Appendix A. Approximate solutions

Here we provide the details of the approximate solutions described in Section §4, for the one and two solubility models.

Appendix A.1. Single solubility model

We start by defining $\delta = 1 - R_c \ll 1$ and rewrite $R = 1 - \delta\bar{R}$. In non-dimensional form $R \in [R_c, 1]$ and so $\bar{R} \in [0, 1]$. Equation (20) becomes

$$\delta \frac{\partial \bar{R}}{\partial t} = 1 - c. \quad (\text{A.1})$$

Equation (A.1) indicates that to leading order $c = 1$. which would correspond to a situation where the fluid has already extracted all the material. This is clearly not the situation when the process starts but we recall that the time scale was chosen for a thickness R_i to be removed.

In this study only a fraction δ is removed, which obviously takes a fraction δ of the time. Consequently we must re-scale time, $\delta\bar{t} = t$, to correctly reflect this, obtaining

$$\frac{\partial\bar{R}}{\partial\bar{t}} = 1 - c, \quad (\text{A.2})$$

$$\frac{\text{Da}}{\delta} \frac{\partial}{\partial\bar{t}}(\epsilon c) + \epsilon_i \frac{\partial c}{\partial x} = \text{Pe}^{-1} \frac{\partial}{\partial x} \left(D \frac{\partial}{\partial x}(\epsilon c) \right) + (1 - \delta\bar{R})(1 - c), \quad (\text{A.3})$$

$$\epsilon = 1 - (1 - \epsilon_i)(1 - \delta\bar{R})^2 = \epsilon_i + 2\delta(1 - \epsilon_i)\bar{R} - (1 - \epsilon_i)\delta^2\bar{R}^2. \quad (\text{A.4})$$

Stage 1. In order to obtain an approximate solution we look for $\bar{R} = R_1 + \mathcal{O}(\delta)$ (i.e. $R = 1 - \delta R_1 + \mathcal{O}(\delta^2)$), $c = c_0 + \delta c_1 + \mathcal{O}(\delta^2)$, so then $\epsilon \sim \epsilon_i + 2\delta(1 - \epsilon_i)R_1 + \mathcal{O}(\delta^2)$. Taking into account that $\text{Da}, \text{Pe}^{-1} \ll \delta$ and balancing the order one and order δ terms in the mass balance and radius equations we obtain

$$\epsilon_i \frac{\partial c_0}{\partial x} = 1 - c_0, \quad \frac{\partial R_1}{\partial\bar{t}} = 1 - c_0, \quad \epsilon_i \frac{\partial c_1}{\partial x} = -R_1(1 - c_0) - c_1. \quad (\text{A.5})$$

These are subject to

$$c_0(0, \bar{t}) = c_1(0, \bar{t}) = R_1(x, 0) = 0, \quad (\text{A.6})$$

such that

$$c_0(x, \bar{t}) = 1 - e^{-x/\epsilon_i}, \quad R_1(x, \bar{t}) = \bar{t}e^{-x/\epsilon_i}, \quad c_1(x, \bar{t}) = (e^{-x/\epsilon_i} - 1)\bar{t}e^{-x/\epsilon_i}. \quad (\text{A.7})$$

Therefore, the approximate solutions in terms of $t = \delta\bar{t}$ read

$$R(x, t) \sim 1 - \delta R_1(x, t) = 1 - te^{-x/\epsilon_i}, \quad (\text{A.8})$$

$$c(x, t) \sim c_0(x, t) + \delta c_1(x, t) = (1 - \exp(-x/\epsilon_i))(1 - e^{-x/\epsilon_i}t). \quad (\text{A.9})$$

The interface between the initial fluid and solvent moves with velocity $u = 1$ (i.e. $u^* = u_i^*$). Hence the above solution holds over the region $x \leq t/\text{Da}$ ($x^* \leq u_i^*t^*$). The solvent reaches the end of the column when $t_1^* = L^*/u_i^*$ or equivalently $t_1 = \mathcal{L}^*L/(u_i^*\tau^*) = L\text{Da}$.

Stage 2. After t_1 equations (A.8)-(A.9) are valid in the whole column provided there is material to extract in the fibers, that is while $R \geq R_c$ everywhere. Since the concentration is lowest at the inlet the radius decreases most rapidly there, consequently we may state that this system is valid provided $R(0, t) \geq R_c$. According to (A.8), to first order,

$$R(0, t) \approx 1 - t, \quad (\text{A.10})$$

which indicates that the solution is valid for $t \leq t_2 = \delta = 1 - R_c$ (at least to $\mathcal{O}(\delta^2)$). We assume that this occurs after the the solvent has first reached the outlet (i.e. $t_2 > t_1$, see section §6). We note that $t_2 = 1 - R_c$ corresponds to $\bar{t} = 1$ which indicates that the time-scale, the time for the radius to reduce from the initial to the final value, is well chosen.

One final restriction is given by the fact that the concentration must be below the saturation value, here scaled to unity. In view of (A.9) this is satisfied for all times. This indicates that even on this slow time-scale the extraction rate is much slower than the flow, so the solvent passes through the column without ever reaching its saturation value.

Stage 3. For $t > 1 - R_c$ extraction occurs beyond some point $x = s(t) > 0$. This is defined as the final point where $R = R_c$ ($\bar{R} = 1$), for $x > s$ the fibres are still coated, $R > R_c$. The position $x = s(t)$ will gradually move along the column as material is removed. Consequently, in terms of the new variable \bar{t} , for $\bar{t} > 1$, we must deal with a moving boundary problem such that for $x \leq s(\bar{t})$

$$c(x, \bar{t}) = 0, \quad \bar{R}(x, \bar{t}) = 1. \quad (\text{A.11})$$

While for $x \geq s(\bar{t})$ equations (A.2-A.4) determine the variables. At the moving interface continuity of flux requires $c(s(\bar{t}), \bar{t}) = 0 + \mathcal{O}(\text{Pe}^{-1})$ and continuity of the radius $\bar{R}(s(\bar{t}), \bar{t}) = 1$.

To deal with the moving boundary we switch to a coordinate system moving with the boundary, $\eta = x - s(\bar{t})$, and seek a travelling wave form. In terms of the new co-ordinate we define concentration and radius functions $c(x, \bar{t}) = f(\eta)$, $\bar{R}(x, \bar{t}) = g(\eta)$, where $f(0) = 0$, $g(0) = 1$. Sufficiently far ahead of the boundary $\eta \rightarrow \infty$ the solvent is saturated and no material is being extracted, $f = 1$, $g = 0$. (Note, this is a theoretical point, complete saturation occurs far past the end of the column as $x \rightarrow \infty$ but it is required for the mathematical solution. This does not affect the validity of the result, but is required to ascertain the velocity.)

Expanding $f(\eta) \sim f_0(\eta) + \delta f_1(\eta) + \dots$, $g(\eta) \sim g_1(\eta) + \dots$ and substituting in (A.2)-(A.4) the leading and first order terms satisfy

$$\epsilon_i \frac{\partial f_0}{\partial \eta} = 1 - f_0, \quad -\frac{ds}{d\bar{t}} \frac{\partial g_1}{\partial \eta} = 1 - f_0 = \epsilon_i \frac{\partial f_0}{\partial \eta}, \quad \epsilon_i \frac{\partial f_1}{\partial \eta} = -g_1(1 - f_0) - f_1, \quad (\text{A.12})$$

where $f_0(0) = f_1(0) = 0$, $g_1(0) = 1$. A strong restriction to travelling wave forms is that the speed $ds/d\bar{t} = v$ is constant, this may only be verified once a solution is obtained. Integrating and applying the boundary conditions gives

$$f_0 = 1 - e^{-\eta/\epsilon_i}, \quad (\text{A.13})$$

$$f_1 = \left[\frac{\epsilon_i}{v} (e^{-\eta/\epsilon_i} - 1) - \frac{v - \epsilon_i}{\epsilon_i v} \eta \right] e^{-\eta/\epsilon_i}, \quad g_1 = 1 - \frac{\epsilon_i}{v} (1 - e^{-\eta/\epsilon_i}). \quad (\text{A.14})$$

In the far-field, $\eta \rightarrow \infty$, the fluid is saturated and we see that $f \rightarrow 1$ is automatically satisfied by the above solution. The condition on the radius $\bar{R} \rightarrow 0$ requires $g_1 \rightarrow 0$. This determines the velocity $v = \epsilon_i$ and so

$$f_1 = (e^{-\eta/\epsilon_i} - 1) e^{-\eta/\epsilon_i}, \quad g_1 = e^{-\eta/\epsilon_i}. \quad (\text{A.15})$$

The fact that we have found a consistent solution indicates that the supposition of constant speed $v = \epsilon_i$ was correct. Then, since $ds/d\bar{t} = v$, we may now write $s(\bar{t}) = \epsilon_i(\bar{t} - 1)$, after applying $s(1) = 0$. To summarize, the solution in this third stage in terms of t is given by

$$\begin{aligned} c(x, t) &\sim (1 - e^{-x/\epsilon_i} e^{(t/\delta - 1)}) (1 - \delta e^{-x/\epsilon_i} e^{(t/\delta - 1)}), \\ R(x, t) &\sim 1 - \delta e^{-x/\epsilon_i} e^{(t/\delta - 1)}, \end{aligned} \quad (\text{A.16})$$

provided

$$x \geq s(t) = \frac{\epsilon_i}{1 - R_c} (t - 1 + R_c),$$

while for $x < s(t)$ it is simply given by $R(x, t) = R_c$ and $c(x, t) = 0$.

This solution holds until the wave reaches the end of the column, $x = L$. Hence, we define the end of the process as the time t_f in which the wave reaches the outlet, that is $s(t_f) = L$ that is given by

$$t_f = (1 - R_c) \left(\frac{1}{\epsilon_i} + 1 \right).$$

Appendix A.2. Model for two distinct solubilities

We now consider the case where the material to be extracted has two distinct solubilities with the switch occurring when $R = R_w$ (i.e. $\bar{R} = (1 - R_w)/(1 - R_c)$). The reduced forms of (A.2) and (A.3) may be written

$$\frac{\partial \bar{R}}{\partial \bar{t}} = \chi - c, \quad \epsilon_i \frac{\partial c}{\partial x} = (1 - \delta \bar{R})(\chi - c), \quad (\text{A.17})$$

where

$$\chi = \begin{cases} c_w & \text{if } \bar{R} \geq (1 - R_w)/(1 - R_c) \\ 1 & \text{if } \bar{R} < (1 - R_w)/(1 - R_c) \end{cases}. \quad (\text{A.18})$$

Stages 1 and 2. Until the radius at $x = 0$ reaches the switching value, R_w , the process involves a single solubility material and so is identical to that studied in Appendix A.1. Hence the radius and concentration are defined by (A.8, A.9) and the only difference is that Stage 2 ends when $R(0, t_2) = R_w$, ($\bar{R}(0, \bar{t}) = (1 - R_w)/(1 - R_c)$). From equation (A.8) we find

$$t_2 = 1 - R_w. \quad (\text{A.19})$$

Stage 3. For $t > t_2$ extraction occurs with two different solubilities. We define the interface by $x = s_1(t)$ such that $R(s_1(t), t) = R_w$ and for $x < s_1(t)$, $\chi = c_w$ while for $x > s_1(t)$, $\chi = 1$.

Again we seek a travelling wave form and so introduce the moving coordinate $\eta = x - s_1(\bar{t})$ such that $v_1(\bar{t}) = ds_1/d\bar{t}$. As before we seek solutions of the form $c(x, \bar{t}) = f(\eta)$ and $\bar{R}(x, \bar{t}) = g(\eta)$ with the conditions that $f(0) = c(s_1(\bar{t}), \bar{t}) = A$, where A is an unknown constant, and $g(0) = \bar{R}(s_1(\bar{t}), \bar{t}) = (1 - R_w)/(1 - R_c)$. Expanding again in powers of δ leads to

$$\epsilon_i \frac{\partial f_0}{\partial \eta} = \chi - f_0, \quad -v_1 \frac{\partial g_1}{\partial \eta} = \chi - f_0, \quad \epsilon_i \frac{\partial f_1}{\partial \eta} + f_1 = -g_1(\chi - f_0), \quad (\text{A.20})$$

with initial conditions given by $f_0(0) = A$, $f_1(0) = 0$ and $g_1(0) = (1 - R_w)/(1 - R_c)$, and

$$\chi = \begin{cases} c_w & \text{if } \eta \leq 0 \\ 1 & \text{if } \eta > 0 \end{cases}. \quad (\text{A.21})$$

The appropriate solutions are

$$f_0(\eta) = \chi + (A - \chi)e^{-\eta/\epsilon_i}, \quad (\text{A.22})$$

$$g_1(\eta) = \frac{1 - R_w}{1 - R_c} + \frac{\epsilon_i}{v_1}(A - \chi)(1 - e^{-\eta/\epsilon_i}), \quad (\text{A.23})$$

$$f_1(\eta) = \frac{A - \chi}{\epsilon_i} \left[\left(\frac{\epsilon_i}{v_1}(A - \chi) + \frac{1 - R_w}{1 - R_c} \right) \eta - \frac{\epsilon_i^2}{v_1}(A - \chi)(1 - e^{-\eta/\epsilon_i}) \right] e^{-\eta/\epsilon_i}. \quad (\text{A.24})$$

To determine v_1 and A we first note that sufficiently far ahead the concentration must approach its saturation value and so there can be no erosion, $c = R = 1$. The condition $c = 1$ is automatically satisfied as $\eta \rightarrow \infty$ while $R = 1$ ($\bar{R} = 0$) requires $g(\eta) \rightarrow 0$ as $\eta \rightarrow \infty$. This gives

$$\frac{1 - R_w}{1 - R_c} + \frac{\epsilon_i}{v_1}(A - 1) = 0. \quad (\text{A.25})$$

A second necessary condition may be found by assuming the solution is bounded at either end. As $\eta \rightarrow \infty$ it is already bounded by $c = R = 1$. A long way downstream, $\eta \rightarrow -\infty$ the negative exponential would blow up unless $A = \chi = c_w$ (which removes the exponential terms from f_0, f_1, g_1) and then from (A.25)

$$v_1 = \epsilon_i(1 - c_w) \frac{1 - R_c}{1 - R_w}. \quad (\text{A.26})$$

Substituting for A, v_1, χ we now obtain

$$f_0(\eta) = \begin{cases} c_w & \text{if } \eta < 0 \\ 1 - (1 - c_w)e^{-\eta/\epsilon_i} & \text{if } \eta \geq 0 \end{cases}, \quad (\text{A.27})$$

$$g_1(\eta) = \begin{cases} (1 - R_w)(1 - R_c)^{-1} & \text{if } \eta < 0 \\ (1 - R_w)(1 - R_c)^{-1}e^{-\eta/\epsilon_i} & \text{if } \eta \geq 0 \end{cases}, \quad (\text{A.28})$$

$$f_1(\eta) = \begin{cases} 0 & \text{if } \eta < 0 \\ -(1 - c_w)(1 - R_w)(1 - R_c)^{-1} (1 - e^{-\eta/\epsilon_i}) e^{-\eta/\epsilon_i} & \text{if } \eta \geq 0 \end{cases}. \quad (\text{A.29})$$

Obviously, in reality the column has finite length. The mathematical artifice of imposing infinite boundaries therefore introduces an error which depends on the size of the exponential. If we were to impose the condition $f = 0$ at the inlet, $\eta = -s_1$, and consider just the leading order then $f_0(-s_1) = 0$ requires $A = c_w(1 - e^{-s_1(t)/\epsilon_i})$. This indicates that A in fact varies with time (which is not permitted under the travelling wave assumption) by neglecting this the error in our solution is of the order $e^{-s_1(t)/\epsilon_i}$. So the error due to setting the boundary at negative infinity is greatest when s_1 is close to zero (in fact $s_1 = 0$ marks the transition from one state to another and we should expect the travelling wave to fail here) but decreases exponentially with increasing s_1 . The constant values of the concentration and radius (to this order) for $\eta \leq 0$ are also a consequence of the boundary position. The fluid has had plenty of time to reach its saturation value. In general $c_w \ll c_s$ so again the error is small, in §6 we see that $c_w \sim 0.1c_s$ so we may expect maximum errors of the order 10%. But again this decreases exponentially with s_1 .

Stage 3 finishes when the wave reaches the column exit. Noting that

$$s_1 = v_1(\bar{t} - \bar{t}_2) = \frac{v_1}{\delta}(t - t_2) \quad (\text{A.30})$$

and applying $s(t_3) = L$ requires

$$t_3 = (1 - R_w) \left(1 + \frac{L}{\epsilon_i(1 - c_w)} \right). \quad (\text{A.31})$$

Note, a second possible scenario is that the inlet material is stripped before this wave reaches the outlet. In the case where $c_w \ll c_s$ this is unlikely to happen but in other situations it may be possible. The above solution will not capture this form. A different form of analysis would then be required to deal with the inlet region and match this to the travelling wave. Here, we use the above solution.

Stage 4. In this stage we seek a travelling wave modelling the removal of the second lanolin layer. This final stage has two distinct components. First, material is removed throughout the

column until $R(0, t) = R_c$, subsequently we have a new moving front problem where the core is slowly stripped and the process ends.

With the current level of approximation, at the start of Stage 4 the radius is R_w everywhere. So during this stage we may proceed as in Stage 2 for the single solubility model to find the first order solutions

$$c(x, t) = c_w(1 - e^{-x/\epsilon_i}), \quad R(x, t) = R_w - c_w(t - t_3)e^{-x/\epsilon_i}. \quad (\text{A.32})$$

The material at the inlet is completely eroded when $R(0, t_4) = R_c$, so

$$t_4 = t_3 + \frac{R_w - R_c}{c_w} = (1 - R_w) \left(1 + \frac{L}{\epsilon_i(1 - c_w)} \right) + \frac{R_w - R_c}{c_w}. \quad (\text{A.33})$$

Stage 5. This stage deals with the final stripping process, which has a moving front defined by $R(s_2(t), t) = R_c$ (with $s_2(t_4) = 0$). This analysis follows almost exactly that of Stage 3 for the single solubility model, with a slight change in notation. Introducing the new travelling wave co-ordinate $\zeta = x - s_2(\bar{t})$ (and working in the \bar{t} time-scale) we write $c(x, \bar{t}) = f(\zeta) = f_0(\xi) + \delta f_1(\zeta) + \dots$ and $\bar{R}(x, \bar{t}) = g(\zeta) = g_1(\zeta) + \dots$. This leads to

$$\epsilon_i \frac{\partial f_0}{\partial \zeta} = c_w - f_0, \quad -v_2 \frac{\partial g_1}{\partial \zeta} = c_w - f_0, \quad \epsilon_i \frac{\partial f_1}{\partial \zeta} = -g_1(c_w - f_0) - f_1 \quad (\text{A.34})$$

where $v_2 = ds_2/d\bar{t}$. These are subject to $f_0(0) = f_1(0) = 0$ (the solvent is clean before the front is reached) and $g_1(0) = 1$ (the fibres have reached its core radius, R_c). In the far-field, $\zeta \rightarrow \infty$ we have $g_1 \rightarrow (1 - R_w)/(1 - R_c)$ to determine the velocity.

Following the analysis of Stage 3 single solubility determines

$$v_2 = \frac{1 - R_c}{R_w - R_c} c_w \epsilon_i, \quad (\text{A.35})$$

and so

$$s_2(t) = \frac{t - t_4}{R_w - R_c} c_w \epsilon_i. \quad (\text{A.36})$$

To leading order

$$c(x, t) \sim c_w(1 - e^{-(x-s_2(t))/\epsilon_i}), \quad (\text{A.37})$$

$$R(x, t) \sim R_c + (R_w - R_c)(1 - e^{-(x-s_2(t))/\epsilon_i}), \quad (\text{A.38})$$

and the process ends when $s_2(t_f) = L$ such that

$$t_f = (1 - R_w) \left(1 + \frac{L}{\epsilon_i(1 - c_w)} \right) + \frac{R_w - R_c}{c_w} \left(1 + \frac{L}{\epsilon_i} \right). \quad (\text{A.39})$$

References

- [1] Z. Huang, X.-H. Shi, W.-J. Jiang, Theoretical models for supercritical fluid extraction, *Journal of Chromatography A* 1250 (2012) 2–26.
- [2] F. Bakkali, S. Averbeck, D. Averbeck, M. Idaomar, Biological effects of essential oils – A review, *Food and Chemical Toxicology* 46 (2) (2008) 446–475.
- [3] B. Sanda, I. Liliana, Natural dye extraction and dyeing of different fibers: a review, John Wiley & Sons, Ltd, 2021, Ch. 4, pp. 113–135.
- [4] Q.-W. Zhang, L.-G. Lin, W.-C. Ye, Techniques for extraction and isolation of natural products: A comprehensive review, *Chinese Medicine* 13 (1) (2018) 1–26.
- [5] J. Thewlis, Lanolin for cosmetic applications, *Agro Food Industry Hi-Tech* May/June (1977) 14–20.
- [6] Lanolin, <https://en.wikipedia.org/wiki/Lanolin#Applications>, last accessed: 04-10-2021.
- [7] H. Sovová, Rate of the vegetable oil extraction with supercritical carbon dioxide - i. modelling of extraction curves, *Chemical Engineering Science* 49 (3) (1994) 409–414.
- [8] M. McHugh, V. Krukonis, H. Brenner, *Supercritical Fluid Extraction: Principles and Practice*, Butterworth-Heinemann series in chemical engineering, Elsevier Science, 2013.
- [9] J. DeSimone, W. Tumas, *Green Chemistry Using Liquid and Supercritical Carbon Dioxide*, Green Chemistry, Oxford University Press, 2003.
- [10] C.-H. Cheng, T.-B. Du, H.-C. Pi, S.-M. Jang, Y.-H. Lin, H.-T. Lee, Comparative study of lipid extraction from microalgae by organic solvent and supercritical CO₂, *Bioresource Technology* 102 (21) (2011) 10151–10153.
- [11] A. Rajaei, M. Barzegar, Y. Yamini, Supercritical fluid extraction of tea seed oil and its comparison with solvent extraction, *European Food Research and Technology* 220 (3) (2005) 401–405.
- [12] Z. Xu, J. Godber, Comparison of supercritical fluid and solvent extraction methods in extracting γ -oryzanol from rice bran, *Journal of the American Oil Chemists' Society* 77 (5) (2000) 547–551.
- [13] T. Veress, Sample preparation by supercritical fluid extraction for quantification a model based on the diffusion-layer theory for determination of extraction time, *Journal of Chromatography A* 668 (2) (1994) 285–291.
- [14] E. Reverchon, J. Daghero, C. Marrone, M. Mattea, M. Poletto, Supercritical fractional extraction of fennel seed oil and essential oil: experiments and mathematical modeling, *Industrial & Engineering Chemistry Research* 38 (8) (1999) 3069–3075.
- [15] M. Perrut, J. Clavier, M. Poletto, E. Reverchon, Mathematical modeling of sunflower seed extraction by supercritical CO₂, *Industrial & engineering chemistry research* 36 (2) (1997) 430–435.

- [16] H. Sovová, Mathematical model for supercritical fluid extraction of natural products and extraction curve evaluation, *The Journal of Supercritical Fluids* 33 (1) (2005) 35–52.
- [17] B. Roy, M. Goto, T. Hirose, Extraction of ginger oil with supercritical carbon dioxide: experiments and modeling, *Industrial & Engineering Chemistry Research* 35 (2) (1996) 607–612.
- [18] A. Valverde, J. Alvarez-Florez, F. Recasens, Mathematical modelling of supercritical fluid extraction of liquid lanolin from raw wool. Solubility and mass transfer rate parameters, *Chemical Engineering Research and Design* 164 (2020) 352–360.
- [19] A. Valverde, F. Recasens, Extraction of solid lanoline from raw wool with near-critical ethanol modified CO₂ – A mass transfer model, *The Journal of Supercritical Fluids* 145 (2019) 151–161.
- [20] J. Park, O. Levenspiel, The crackling core model for the reaction of solid particles, *Chemical Engineering Science* 30 (10) (1975) 1207–1214.
- [21] M. Goto, B. Roy, T. Hirose, Shrinking-core leaching model for supercritical-fluid extraction, *The Journal of Supercritical Fluids* 9 (2) (1996) 128–133.
- [22] O. Levenspiel, *Chemical Reaction Engineering*, 3rd Edition, John Wiley & Sons, Inc., 1999.
- [23] L. Fiori, D. Basso, P. Costa, Supercritical extraction kinetics of seed oil: A new model bridging the ‘broken and intact cells’ and the ‘shrinking-core’ models, *The Journal of Supercritical Fluids* 48 (2009) 131–138.
- [24] A. Rai, K. D. Punase, B. Mohanty, R. Bhargava, Evaluation of models for supercritical fluid extraction, *International Journal of Heat and Mass Transfer* 72 (2014) 274–287.
- [25] H. Patel, Fixed bed column adsorption study: a comprehensive review, *Applied Water Science* 9 (45) (2019).
- [26] M. J. Ahmed, B. H. Hameed, Removal of emerging pharmaceutical contaminants by adsorption in a fixed-bed column, *Ecotoxicology and Environmental Safety* 149 (2018) 257–266.
- [27] T. G. Myers, F. Fon, M. G. Hennessy, Mathematical modelling of carbon capture in a packed column by adsorption, *Applied Energy* 278 (2020) 115565.
- [28] T. G. Myers, F. Font, Mass transfer from a fluid flowing through a porous media, *International Journal of Heat and Mass Transfer* 163 (2020) 120374.
- [29] V. Eychenne, S. Sáiz, F. Trabelsi, F. Recasens, Near-critical solvent extraction of wool with modified carbon dioxide - experimental results, *The Journal of Supercritical Fluids* 21 (2001) 23–31.
- [30] W. S. Simpson, G. Crawshaw, *Wool: Science and Technology*, Woodhead Publishing Series in Textiles, Elsevier, 2002.

- [31] A. T. King, The specific gravity of wool and its relation to swelling and sorption in water and other liquids, *Journal of the Textile Institute Transactions* 17 (1) (1926) T53–T67.
- [32] P. R. Fields, T. L. Chester, A. M. Stalcup, Viscosity estimation in binary and ternary supercritical fluid mixtures containing carbon dioxide using a supercritical fluid chromatograph, *Journal of Liquid Chromatography & Related Technologies* 34 (2011) 995–1003.
- [33] K. Abaroudi, F. Trabelsi, B. Calloud-Gabriel, F. Recasens, Mass transport enhancement in modified supercritical fluid, *Industrial & Engineering Chemistry Research* 38 (1999) 3505–3518.
- [34] J. Puiggené, M. A. Larrayoz, F. Recasens, Free liquid-to-supercritical fluid mass transfer in packed beds, *Chemical Engineering Science* 52 (2) (1997) 195–212.
- [35] C.-S. Tan, S.-K. Liang, D.-C. Liou, Fluid-solid mass transfer in a supercritical fluid extractor, *Chemical Engineering Journal* 38 (1) (1988) 17–22.